



HAL
open science

Combining chemistry and topography to produce antifouling surfaces, a review

Hippolyte Durand, Amelia Whiteley, Pascal Mailey, Guillaume Nonglaton

► **To cite this version:**

Hippolyte Durand, Amelia Whiteley, Pascal Mailey, Guillaume Nonglaton. Combining chemistry and topography to produce antifouling surfaces, a review. *ACS Applied Bio Materials*, 2022, 5 (10), pp.4718-4740. 10.1021/acsabm.2c00586 . cea-03949689

HAL Id: cea-03949689

<https://cea.hal.science/cea-03949689v1>

Submitted on 20 Jan 2023

HAL is a multi-disciplinary open access archive for the deposit and dissemination of scientific research documents, whether they are published or not. The documents may come from teaching and research institutions in France or abroad, or from public or private research centers.

L'archive ouverte pluridisciplinaire **HAL**, est destinée au dépôt et à la diffusion de documents scientifiques de niveau recherche, publiés ou non, émanant des établissements d'enseignement et de recherche français ou étrangers, des laboratoires publics ou privés.

This document is confidential and is proprietary to the American Chemical Society and its authors. Do not copy or disclose without written permission. If you have received this item in error, notify the sender and delete all copies.

**Combining topography and chemistry to produce
antibiofouling surfaces – a review**

Journal:	<i>ACS Applied Bio Materials</i>
Manuscript ID	mt-2022-00586q.R2
Manuscript Type:	Review
Date Submitted by the Author:	n/a
Complete List of Authors:	Durand, Hippolyte; CEA Tech Leti, DTBS Whiteley, Amelia; CEA Tech Leti, DTBS Mailley, Pascal; CEA, Nonglaton, Guillaume; CEA Tech Leti, DTBS

SCHOLARONE™
Manuscripts

1
2
3
4
5
6
7 1 Combining topography and chemistry to produce
8
9
10
11 2 antibiofouling surfaces – a review
12
13
14
15

16 3 *AUTHORS.*
17
18
19

20 4 *Hippolyte Durand^{‡*}, Amelia Whiteley[‡], Pascal Mailley, Guillaume Nonglaton*
21
22
23
24

25 5
26
27
28

29 6 *ADRESS.*
30
31
32

33 7 Univ. Grenoble Alpes, CEA, LETI, DTBS, F-38000 Grenoble
34
35
36

37 8
38
39

40 9 *KEYWORDS.*
41
42
43

44
45 10 Antibiofouling, antibacterial, topography, surface chemistry, hydrophobic surfaces, hydrophilic
46
47
48 11 surfaces
49
50
51
52
53
54
55
56
57
58
59
60

1
2
3
4 12 ABSTRACT. Despite decades of research on the reduction of surface fouling from biomolecules
5
6
7 13 or micro-organisms, the ultimate antibiofouling surface remains undiscovered. The recent covid-
8
9
10 14 19 pandemic strengthened the crucial need for such treatments. Among the numerous approaches
11
12
13 15 that are able to provide surfaces with antibiofouling properties, chemical, biological and
14
15
16
17 16 topographical strategies have been implemented for instance in marine, medical or food industries.
18
19
20 17 However, many of these methods have a biocidal effect and, with antibioresistance and biocide
21
22
23 18 resistance a growing threat on humanity, strategies based on reducing adsorption of biomolecules
24
25
26
27 19 and micro-organism are necessary for long-term solutions. Bio-inspired strategies, combining both
28
29
30 20 surface chemistry and topography, are currently at the heart of the best innovative and sustainable
31
32
33 21 solutions. The synergistic effect of micro/nano-structuration, together with engineered chemical or
34
35
36
37 22 biological functionalization is believed to contribute to the development of antibiofouling surfaces.
38
39
40 23 This review aims to present approaches combining hydrophobic or hydrophilic chemistries with a
41
42
43
44 24 specific topography to avoid biofouling in various industrial environments and healthcare facilities.
45
46
47

48 25 Contents

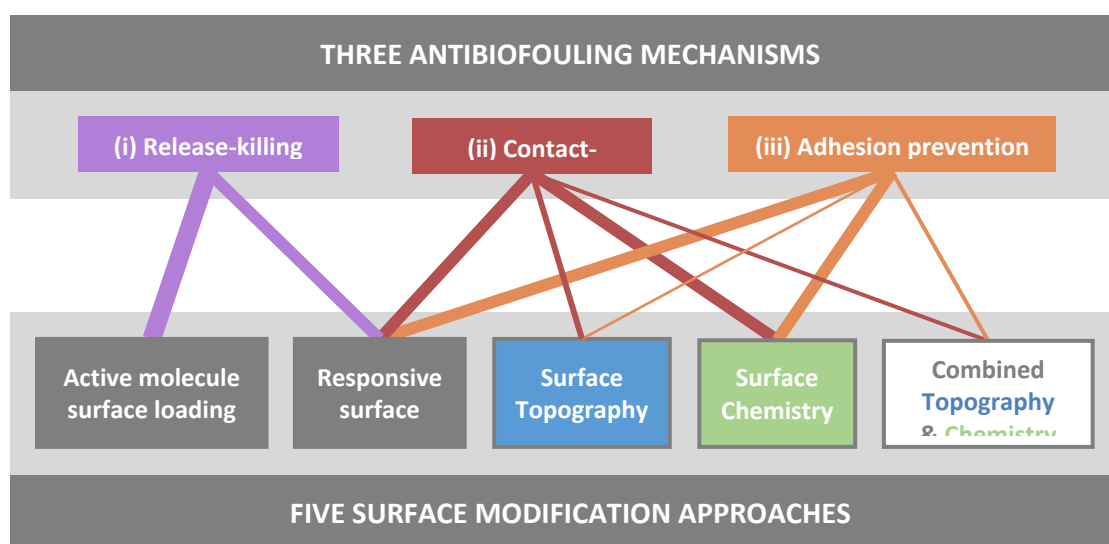
49 26	1. Introduction	4
50 27	2. Combined topography and hydrophobicity for adhesion prevention	12
51 28	2.1. Metallic substrates	13

1			
2			
3			
4	29	2.1.1. Endogenous topography: micro/nanostructure designed from the metallic substrate	
5	30	13	
6			
7	31	2.1.1.1. Aqueous phase treatment.....	14
8			
9	32	2.1.1.2. Laser etching.....	18
10			
11	33	2.1.1.3. Reactive ion etching.....	21
12			
13	34	2.1.2. Exogenous topography: micro/nanostructure through additive strategies on metals	
14			
15	35	22	
16			
17	36	2.1.2.1. Electro-deposition.....	22
18			
19	37	2.1.2.2. Other methods.....	25
20			
21	38	2.2. Glass and silicon substrates	29
22			
23	39	2.3. Polymer substrates	33
24			
25	40	2.3.1. Endogenous topography: micro/nanostructure designed from polymers	34
26			
27	41	2.3.1.1. Molding.....	34
28			
29	42	2.3.1.2. Plasma treatment.....	35
30			
31	43	2.3.2. Exogenous topography: micro/nanostructure through additive strategies on polymers	
32			
33	44	37	
34			
35	45	2.4. Multi-substrate approaches	41
36			
37	46	3. Combined topography and hydrophilicity for multiple antibiofouling mechanisms	44
38			
39	47	3.1. Metallic substrates	45
40			
41	48	3.2. Glass substrates.....	49
42			
43	49	3.3. Polymer substrates	54
44			
45	50	3.3.1.1. Marine industry.....	54
46			
47	51	3.3.1.2. Water filtration.....	57
48			
49	52	3.3.1.3. Medical devices	63
50			
51	53	4. Conclusion & perspectives	66
52			
53	54		
54			
55			
56			
57			
58			
59			
60			

1. Introduction

Surface fouling is defeating man-made devices in various fields. Water treatment¹, marine^{2,3} and food industry⁴ as well as the medical field⁵⁻⁷ are seeking for surfaces that will prevent undesired fouling. This spontaneous deposition of molecules, macromolecules and micro-organisms on an engineered surface upon contact with a liquid medium leads to the formation of biofilms that strongly impede performance and functionality. The predominant use of curative approaches, such as antibiotics in the medical field, or biocides in marine environments, is no longer desirable. Throughout decades of massive administration of antibiotics to human and animal feedstock, more and more resistant bacterial strains have emerged and spread all over the globe. World Health Organization (WHO) recently labelled the arising antibioresistance as the most urgent health threat of our time.⁸ And the European Commission forecasts no less than 10 million deaths per year attributed to antibioresistance in 2050 if today's tendency is not hampered.⁹ Biocide resistance is also on the rise¹⁰ and the important use of tributyltin since the 1960's has caused tremendous damage to the marine environment.^{11,12} Since its prohibition in 2008, more environmentally friendly solutions have been investigated. The scientific community is putting in tremendous efforts in the search for alternative strategies that do not rely only on curative approaches. Their

1
2
3
4 71 focus is now rather on preventive approaches which tackle the initial steps of biofilm development:
5
6
7 72 the adsorption of biomolecules and subsequent micro-organisms adhesion. In this manuscript, the
8
9
10 73 term *antibiofouling* describes the ability of a surface to impede fouling from biological molecules,
11
12
13 74 macro-molecules and/or micro-organisms, while *antifouling* is used for general fouling with any
14
15
16
17 75 type of chemical substance or particle, including inorganic structures. Preventive approaches to
18
19
20 76 fight surface fouling are now predominantly investigated and can be classified according to three
21
22
23 77 different mechanisms: (i) active molecule-releasing and (ii) contact-killing surfaces, that prevent
24
25
26
27 78 micro-organism growth both on and near surfaces, and (iii) anti-adhesive surfaces that prevent
28
29
30 79 molecule, macromolecule and micro-organisms adhesion. These three antibiofouling mechanisms
31
32
33
34 80 can be achieved with five different types of surface modification, as detailed in Figure 1.



81

1
2
3 82 *Figure 1: Three antibiofouling mechanisms linked to corresponding types of surface modification. The*
4 83 *thickness of the links gives an estimation of the amount of research articles on the topics.*

5
6 84 (i) In order to fight surface fouling with a limited quantity of antibiotics or biocides, a first
7
8
9
10 85 mechanism is active molecule releasing-surfaces. Antibiotic and biocide release will kill the micro-
11
12
13 86 organisms before they reach the surface and form biofilms. The release can be spontaneous in
14
15
16 87 *active molecule surface loading* approaches, or triggered by a specific physico-chemical stimuli
17
18
19
20 88 (pH, temperature, UV irradiation, enzymatic activity...) in *responsive surface* approaches.
21
22
23 89 However, these approaches are limited in time, only affect micro-organisms and do not prevent
24
25
26
27 90 biomolecular fouling, and still face the issue of antibioresistance, biocide resistance and damage to
28
29
30 91 the environment. Only short term specific applications will benefit from this mechanism.^{3,13,14}

31
32
33
34 92 (ii). A second mechanism relies on contact-killing. *Surface chemistry* approaches allow
35
36
37 93 immobilization of active molecules onto the surface, leading to micro-organisms being killed upon
38
39
40
41 94 contact or adhesion. In *responsive surface* approaches, the immobilized active molecule action can
42
43
44 95 be triggered upon a specific physico-chemical stimuli. Some responsive surfaces are also able to
45
46
47
48 96 eliminate the accumulation of dead cells that would progressively impede their contact-killing
49
50
51 97 effect. But this contact-killing effect can also be obtained without the use of active molecules.
52
53
54 98 Inspired by numerous natural surfaces in plants and the animal kingdom, engineered surface
55
56
57
58
59
60

1
2
3
4 99 topography (nanopillars, microblades, nanospikes...) is able to, in some cases, cause mechanical
5
6
7 100 stress on adhered micro-organisms, leading to membrane failure and eventually cell death.¹⁵⁻¹⁷
8
9

10 101 Hence, *combined surface topography and chemistry* approaches are also able to achieve contact-
11
12
13 102 killing mechanism, with potential synergistic effects that are reviewed in this manuscript.
14
15
16

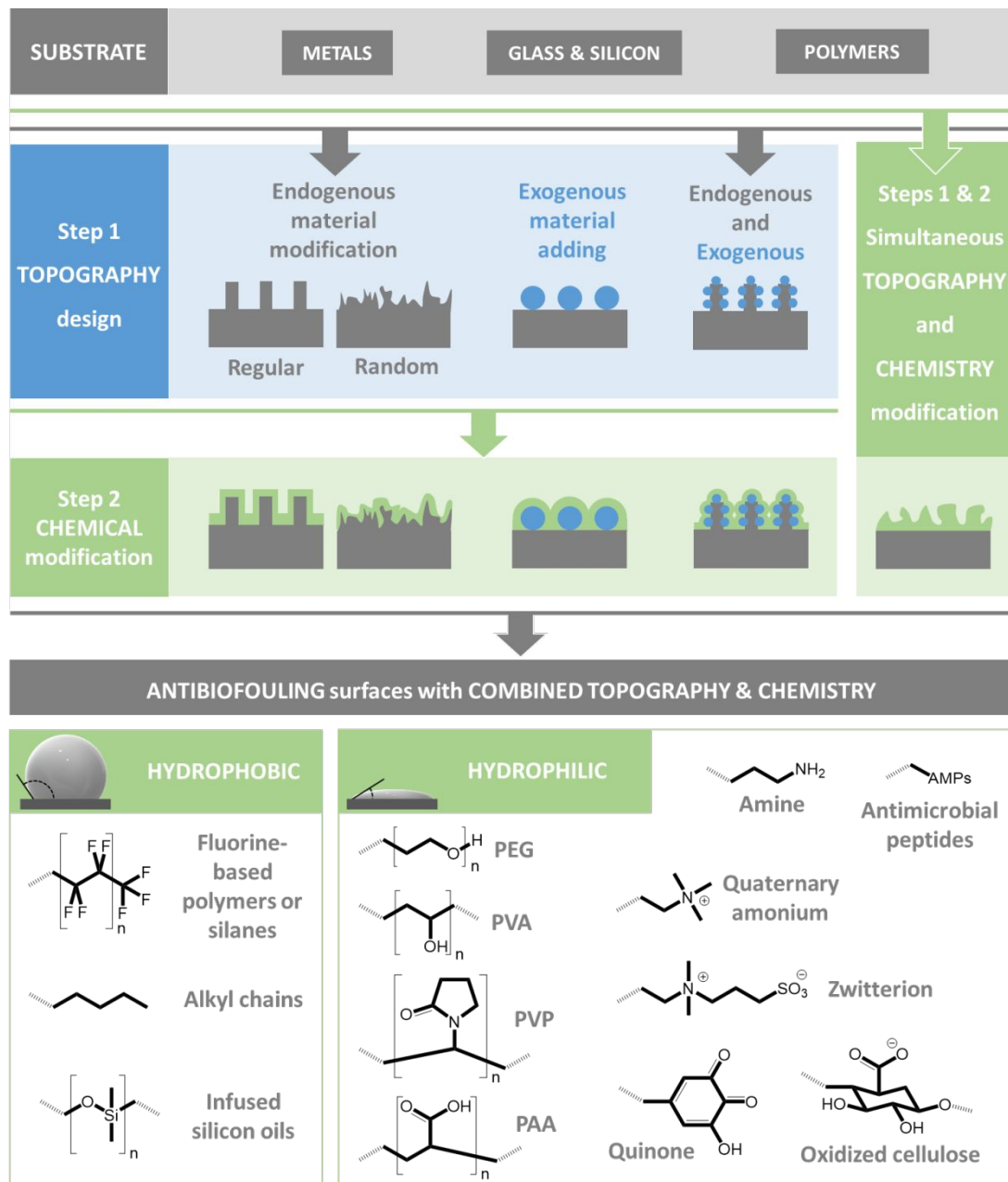
17 103 (iii). At last, only the adhesion prevention mechanism prevents both biomolecules and micro-
18
19
20
21 104 organism fouling since they are engineered to prevent the interaction between the foulants and the
22
23
24 105 surface. For instance, superhydrophobic surfaces obtained by *surface chemistry* or *combined*
25
26
27 106 *topography and chemistry* approaches will avoid surface fouling since the foulants are confined to
28
29
30
31 107 the liquid phase which has a limited contact area with the surface. Similarly, zwitterion molecules
32
33
34 108 or polymers can provide surfaces with superhydrophilic properties, forming a dense hydration layer
35
36
37 109 that can also prevent fouling. Plus, depending on physico-chemical stimuli, *responsive surface*
38
39
40
41 110 approaches offer similar adhesion prevention mechanisms.¹⁸⁻²⁰
42
43
44

45 111
46
47
48
49 112 All these surface modifications tune the surface properties in terms of topography and/or chemical
50
51
52
53 113 composition. Moreover, the still on-going study of natural surfaces in plants, insects and the animal
54
55
56
57
58
59
60

1
2
3
4 114 kingdom have revealed numerous natural antibiofouling strategies that rely on the combination of
5
6
7 115 a specific surface topography with a particular surface chemistry. The published literature over the
8
9
10 116 past 5 years offers approximately five hundred reviews on the *antifouling* topic. Within this
11
12
13 117 overwhelming amount of review articles that cover the afore-mentioned antibiofouling
14
15
16
17 118 mechanisms, approximately 60 of them were selected based on their title and abstracts. They were
18
19
20 119 classified in table S1 of the Supporting information, according to the type of surface modification
21
22
23 120 approach detailed in Figure 1 (*active molecule surface loading, surface chemistry, surface*
24
25
26
27 121 *topography, responsive surface* and *combined topography and chemistry*). Less than ten mention
28
29
30 122 *combined topography and chemistry* approaches, and never as the core topic of the review.^{4,21-27}
31
32
33
34 123 Up to our knowledge, none of them specifically focused only on this approach. This manuscript
35
36
37 124 aims to fill this gap and provide these works with their own specific review. However, these
38
39
40 125 research articles are not easily identified since authors do not always indicate the combined aspect
41
42
43
44 126 of their surface modifications. The research projects described in this review were then selected by
45
46
47 127 using three successive filters: firstly, *surface topography* approaches over the last 5 years were
48
49
50 128 explored. Secondly, the articles in which *surface chemistry* was used to complement the *surface*
51
52
53
54 129 *topography* were isolated. And thirdly, only the works that exposed the engineered surfaces to
55
56
57
58
59
60

1
2
3
4 130 biomolecular and/or micro-organisms fouling were selected. Even if they can be sometimes a
5
6
7 131 source of inspiration for developing antibiofouling surfaces, research topics such as anti-corrosion
8
9
10 132 or self-cleaning surfaces, were mainly left aside.

11
12
13
14 133 The in-depth analysis of the selected works led to several levels of classification following a
15
16
17
18 134 bottom-up process, as detailed in Figure 2. The first one is the nature of the substrate that is to be
19
20
21 135 provided with antibiofouling property: metals and their oxides and hydroxides, glass and silicon-
22
23
24 136 based materials, and polymers. Secondly, the articles are classified depending on the method used
25
26
27
28 137 to tune the substrate topography (step 1), either by modifying the substrate itself (endogenous
29
30
31 138 topography), or by using an additive strategy and adding another material (exogenous topography).
32
33
34 139 The third level relates to the surface chemistry modification: a vast majority of approaches
35
36
37
38 140 complement the topography with a chemical layer (step 2), but some approaches simultaneously
39
40
41 141 tune the substrate topography while producing the chemical layer (step 1&2).
42
43
44
45
46
47
48
49
50
51
52
53
54
55
56
57
58
59
60



142
143 *Figure 2: Combining topography and chemistry to obtain antibiofouling surfaces on different substrates*
144 *(metals, glass and silicon, polymers). The first step consists in designing regular or random topography. In*
145 *the second step a specific chemistry is added. It is also possible to obtain topography simultaneously with*
146 *the surface chemistry modification process. In the next figures, the blue overlay will indicate the*
147 *topography design, while the green overlay will indicate the chemistry modification.*

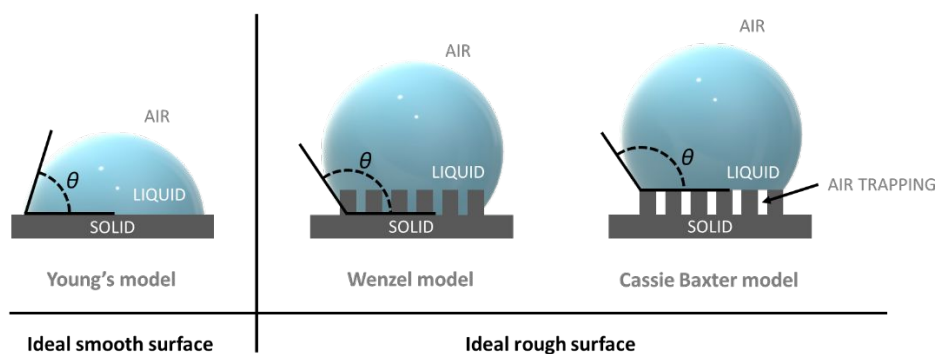
148 Whatever the approach the resulting engineered surface from the combination of topography and
149 chemistry will either fall into hydrophilic or hydrophobic surface. For hydrophobic approaches a

1
2
3
4 150 very limited amount of chemical entities are used: fluorine-based moieties and alkyl chains have
5
6
7 151 been used for a long time in order to produce hydrophobic and superhydrophobic surfaces. More
8
9
10 152 recently, surfaces infused with silicon oils have been developed and used as self-cleaning surfaces
11
12
13 153 (often referred as slippery liquid infused surfaces, SLIS). Some research teams also used them in
14
15
16
17 154 antibiofouling applications. Conversely, for hydrophilic approaches, chemical entities are
18
19
20 155 numerous as exposed on Figure 2. Ranging from simple functional groups such as amine or
21
22
23 156 carboxylic acids to polymers and ionic compounds, hydrophilic approaches are at the heart of
24
25
26
27 157 today's most innovative antibiofouling research works. This manuscript is thus separated into two
28
29
30 158 chapters, the first one detailing the hydrophobic approaches, and the second one focusing on the
31
32
33 159 hydrophilic ones. This review is written from an applicative engineer perspective, the sub-chapters
34
35
36
37 160 are thus organized according to the nature of the surface to be treated: metals, glass and silicon-
38
39
40 161 based or polymers. The conclusion and outlook will provide the reader with recommendations
41
42
43 162 regarding further development of antibiofouling surfaces.

44 45 46 47 163 **2. Combined topography and hydrophobicity for adhesion prevention**

48
49
50
51 164 A majority of topographical hydrophobic approaches use fluorine-based compounds as a chemical
52
53
54
55 165 layer to increase the hydrophobicity. This is why the subchapter will not be organized regarding
56
57
58
59
60

1
2
3
4 166 the type of chemistry used on the engineered surface but rather according to the method of
5
6
7 167 designing the topography: endogenous, exogenous or a combination of both, as detailed on Figure
8
9
10 168 2. Whatever the method, the same objective remains: decrease the contact area between the surface
11
12
13 169 and the liquid medium in order to prevent fouling interactions with biomolecules or micro-
14
15
16
17 170 organisms. As described in Figure 3, different models of surface wetting have been developed and
18
19
20 171 are widely discussed in the literature.^{28,29} The Cassie-Baxter regime is predominantly cited in this
21
22
23 172 sub-chapter since it is the best way to prevent the liquid from fully wetting the surface. This regime
24
25
26
27 173 is almost exclusively reached when a hydrophobic chemical entity is used in combination with the
28
29
30 174 topography design.



175
176 *Figure 3: Surface wetting regimes and contact angle θ measurements on ideal smooth surfaces and*
177 *rough surfaces.*

178 In this chapter, only the production technique of the topographical features really differs from one
179 study to another. This angle is going to lead our story for each category of substrate: metals, silicon-

1
2
3
4 180 based samples and polymers. In addition, a few studies introduce approaches that are compatible
5
6
7 181 with various substrate types. A specific subchapter is dedicated to them. All the approaches are
8
9
10 182 detailed in Table S2 of the Supplementary information.

14 183 **2.1. Metallic substrates**

16
17 184 Metallic surfaces that are potentially exposed to biofouling are encountered in various fields of
18
19
20 185 activity, such as marine industry, food preparation facilities and healthcare.

24 186 **2.1.1. Endogenous topography: micro/nanostructure designed from the** 25 26 187 **metallic substrate**

28
29
30 188 In order to tune the topography, the most straightforward methods rely on the direct modification
31
32
33 189 of the metals surface itself. Micro/nanostructure can be produced through different approaches of
34
35
36 190 aqueous phase treatments and etching techniques which provide the surface with engineered
37
38
39
40 191 topography. These micro/nanostructures are referred as endogenous topographies.

43 192 **2.1.1.1. Aqueous phase treatment**

45
46 193 A simple way to modify the topography of metallic substrates is the formation of oxide and
47
48
49
50 194 hydroxide layers at their surface. Upon immersion in boiling water, acidic or alkaline solutions or
51
52
53 195 a combination of these, metallic oxides, that are produced at the surface of the substrates, form

1
2
3
4 196 hierarchical structures. Aluminium, magnesium or copper substrates are predominantly represented
5
6
7 197 in the following reviewed articles. Using a subsequent step of chemical surface modification with
8
9
10 198 hydrophobic compounds, some research teams managed to use combined topographical and
11
12
13 199 chemical approaches to obtain superhydrophobic substrates. For instance, commercial aluminium
14
15
16
17 200 sheets were enhanced with hierarchical micro/nano topographies produced by strong acid etching
18
19
20 201 followed by immersion in boiling water. Subsequently, 1H,1H,2H,2H-
21
22
23 202 perfluorodecyltrichlorosilane also known as FDTTS was used to chemically functionalize the
24
25
26
27 203 structured Al surfaces, as depicted on Figure 4A.³⁰ During boiling water treatment, the average
28
29
30 204 roughness increased from 5 to 65 nm with the formation of Bohemite under the form of
31
32
33 205 nanoplatelets on top of the existing microprotusions. Only the combination of micro and nanoscale
34
35
36
37 206 roughness with hydrophobic silane grafting provided the surface with superhydrophobic properties
38
39
40 207 which resulted in a drastic decrease of bovine serum albumin (BSA) adsorption. An 80% relative
41
42
43 208 reduction in adhered bacteria was measured, regardless of the bacterial strain and their outer layer
44
45
46
47 209 properties (*Pseudomonas aeruginosa*, *Staphylococcus epidermidis*, and *Staphylococcus aureus*).
48
49
50 210 Finally, cytotoxicity of the samples was assessed through MTT assay and relative complete cell
51
52
53 211 compatibility (HeLa cells) was validated, confirming the benefits of such a treatment for *in vivo*

1
2
3
4 212 applications. More recently, Mandal and co-workers studied the modification of an aluminium
5
6
7 213 alloy through micro-imprinting to obtain square micropillars, followed by hot water treatment
8
9
10 214 which covered the pillars with flake-like AlO(OH) bohemite nanostructures. Finally, a perfluoro-
11
12
13 215 silane layer was deposited by chemical vapor deposition (CVD) on top on the nanostructure. The
14
15
16
17 216 superhydrophobic Cassie-Baxter regime was achieved and allowed for a drastic decrease of
18
19
20 217 *Escherichia coli* growth.^{31,32}
21
22
23

24 218 Copper hydroxide can also be produced to tune the surface topography. A copper mesh was
25
26
27
28 219 modified through the formation of Cu(OH)₂ nanowires at its surface, followed by Cu based metallic
29
30
31 220 organic framework (MOF) production and finally polydimethylsiloxane (PDMS) deposition on the
32
33
34 221 micro/nano structure as depicted in Figure 4B. Hierarchical mushroom-like structures were
35
36
37
38 222 obtained as confirmed by scanning electronic microscopy (SEM) images. Water contact angles
39
40
41 223 above 150° and sliding angles below 4° were measured. Antifouling and self-cleaning properties
42
43
44 224 were validated against products such as, milk, coffee, tea, cola and juice. In addition, dirt and salts
45
46
47
48 225 were easily removed from the substrate leaving no trace. But more importantly, drag reduction also
49
50
51 226 benefited from the treatments applied to the Cu mesh, making it a promising material for innovative
52
53
54 227 marine vehicle development.³³
55
56
57
58
59
60

228

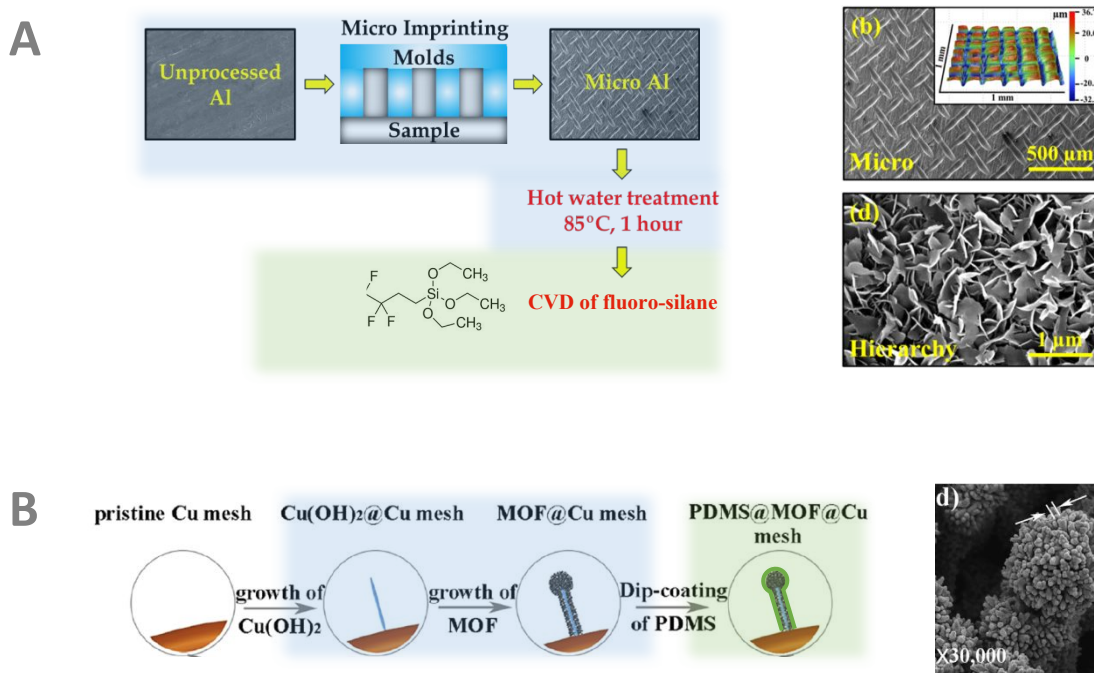


Figure 4: Combined approaches using metal oxide and hydroxide for topography design and detailed surface chemistry adopted. A: Imprinted aluminum micro-pillars covered with bohemite obtained by hot boiling water treatment, followed by FOTES CVD (adapted with permission from reference ³², Copyright 2022 Elsevier), B: super-hydrophobic PDMS/metal-organic-framework copper mesh (adapted with permission from reference ³³, Copyright 2011 Elsevier). Blue and green overlay indicate topography and chemistry modifications, respectively.

2.1.1.2. Laser etching

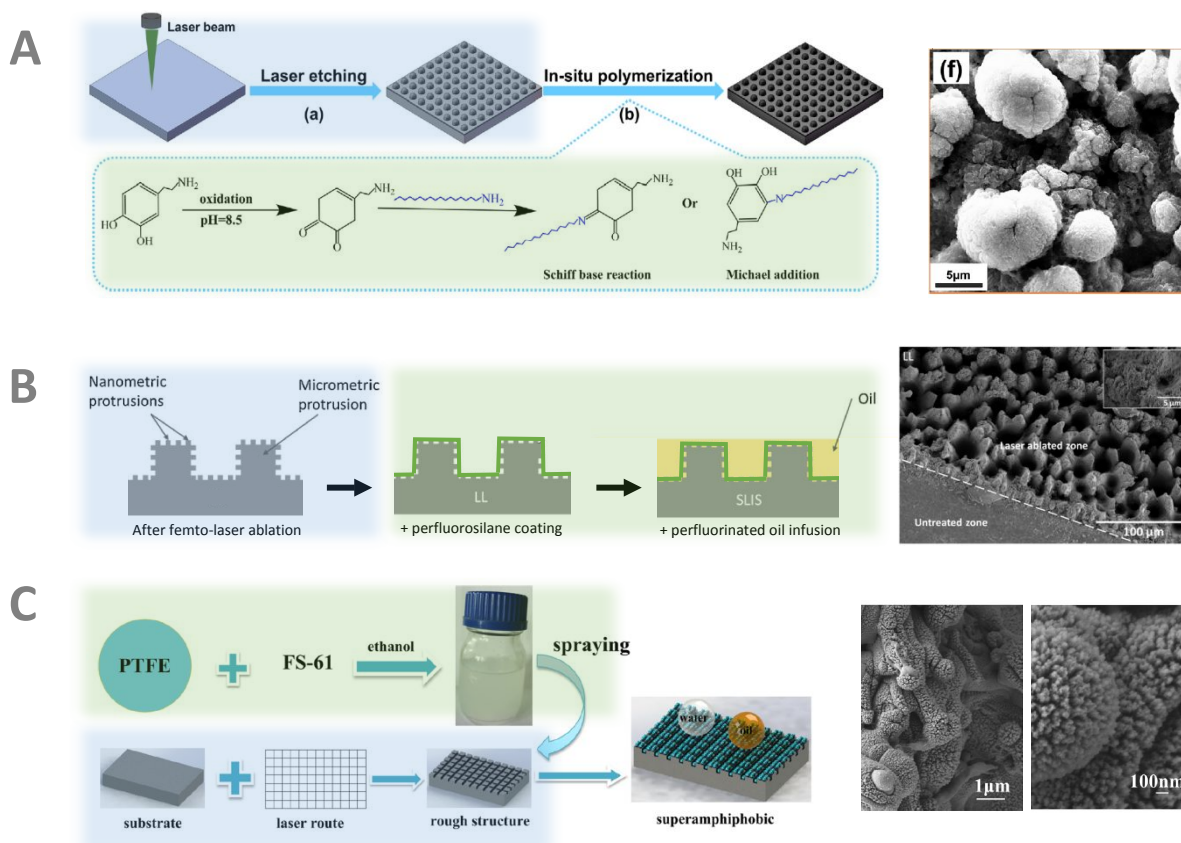
Laser-based techniques are highly represented for modifying metals' topography.^{34,35} Aluminium and stainless steel substrates are easily modified with this technique. For instance, Li *et al* used Laser Interference Patterning on stainless steel to create micro and nano structures mimicking the gecko surface.³⁶ This surface patterning created superhydrophilic substrates with a water contact angle (WCA) close to 0°, in accordance to the Wenzel model (Figure 3). However, the following *in situ* polymerisation of a mixture of polydopamine and octadecylamine monomers led to the

1
2
3
4 243 formation of small flocules and a WCA of 157.3°, confirming superhydrophobicity (see Figure
5
6
7 244 5A). A 1-log reduction of bacterial growth was observed for *E. coli* (about 90% inhibition), a 2-
8
9
10 245 log reduction was obtained against *S. aureus*, for which an inhibition efficacy of over 99% could
11
12
13 246 be observed. The difference in bacterial membrane structure between Gram positive and Gram
14
15
16
17 247 negative is used to explain this result. To assess the long-term use of these substrates, abrasion
18
19
20 248 tests were carried out with sandpaper, and 6-month storage in air also took place. Neither of these
21
22
23
24 249 experiments considerably affected the properties of the surfaces.

25
26
27
28 250 Taking inspiration from lotus leaves, Zouaghi and co-workers used femtosecond laser ablation onto
29
30
31 251 stainless steel surface to produce micro and nano topography. Here, the surface was coated with a
32
33
34 252 perfluorosilane in an organic solvent, resulting in a first combined approach called LL (lotus-
35
36
37
38 253 like).³⁷ A second approach consisted in impregnating this LL substrate with an perfluorinated oil
39
40
41 254 in order to obtain a slippery liquid infused surface (SLIS) also known as SLIPS (for slippery liquid
42
43
44
45 255 infused porous surface), as depicted in

46
47
48
49 256 Figure 5B. Antibiofouling tests were performed in a pilot pasteurizer with a model fluid composed
50
51
52 257 of 1 wt% of whey protein, in a temperature range representing dairy industry conditions (65-85°C).
53
54
55 258 Although a complete suppression of fouling was observed for SLIPS, an increase in fouling was

1
2
3
4 259 detected for LL. The wide open topography of LL substrates explained the fouling increase, large
5
6
7 260 and deep holes of *ca.* 10 to 20 μm were easily filled by foulants and the role of chemical layer was
8
9
10 261 impeded, as explained by the authors.³⁸ The SLIPS substrate benefited from the infused
11
12
13 262 hydrophobic oil which behaved like a smooth liquid surface. However, the SLIPS approach failed
14
15
16
17 263 durability testing after only one cycle in the pasteurizer. An optimized topography to increase oil
18
19
20 264 retention and the use of an alternative oil more suitable to the food industry are cited as
21
22
23
24 265 perspectives.



266

267 *Figure 5: Combined approaches using laser techniques for topography design and detailed surface*
 268 *chemistry adopted. A: Laser Interference Patterning on stainless steel, followed by polymerization of*
 269 *octadecylamine and polydopamine (adapted with permission from reference ³⁶, Copyright 2019 Elsevier).*
 270 *B: femtosecond laser ablation onto stainless steel followed by perfluorosilane coating and perfluorinated*
 271 *oil infusion (adapted with permission from reference ³⁸, Copyright Elsevier 2019).*
 272 *C: UV laser etching on aluminum and stainless steel, coated with PTFE nanoparticles (adapted with permission from reference*
 273 *³⁹, Copyright 2021 Elsevier). Blue and green overlay indicate topography and chemistry modifications,*
 274 *respectively.*

275 Ultraviolet (UV) laser etching was also used on aluminium and stainless steel metallic substrates
 276 to produce topographic features following vertical and horizontal lines with 30 μm spacing. Then,
 277 a coating composed of polytetrafluoroethylene (PTFE) nanoparticles and surfactant was sprayed
 278 with N₂ gas onto the etched metallic surfaces, before a final thermal treatment (Figure 5C). SEM

1
2
3
4 279 imaging revealed the micro and nano-sized topographical features. Chemical characterization with
5
6
7 280 energy dispersive spectroscopy confirmed the homogeneous covering with the spraying technique.
8
9
10 281 The wettability was evaluated against several different liquids (water (pH 0 and 14), ethanol
11
12
13 282 solutions, rapeseed oil, ethylene glycol, propylene glycol and cyclohexane) that all reached contact
14
15
16
17 283 angles above 150°, confirming superamphiphobic properties. The combination of surface
18
19
20 284 topography and hydrophobic chemistry leads to antifouling properties and has potential drag-
21
22
23
24 285 reduction properties. Moreover, the mechanical robustness of the coating was confirmed after
25
26
27 286 abrasion tests which led to a very small loss of super-amphiphobic properties. The micro
28
29
30 287 topography withstood the abrasion and both nano topography and chemical functions were
31
32
33
34 288 preserved.³⁹

37 289 **2.1.1.3. Reactive ion etching**

40 290 Reactive ion etching (RIE) was implemented on stainless steel by Cao and co-workers to produce
41
42
43
44 291 rectangular micropillars with different arrangements and spacing. A peptide coating was applied
45
46
47 292 through immersion, and resulted in a hydrophobic surface that decreased the adhesion of marine
48
49
50 293 algae *Chlorella pyrenoidosa* and *Phaeodactylum tricornutum*. The synergy between topography
51
52
53
54 294 and chemical peptide layer was confirmed.⁴⁰ High power electro-etching in sodium chloride
55
56
57
58
59
60

1
2
3
4 295 solution has also been used to produce micropillars on stainless steel surface, followed by vapor
5
6
7 296 deposition of various FDA-approved food-contact coatings: Ni-P-PTFE, Lectrofluor® 641, CrN,
8
9
10 297 TiN, and Dursan®. Among them, the patented Dursan® coating process offered the most
11
12
13 298 promising fouling resistance against *L. monocytogenes*, but the combination with micropillars gave
14
15
16
17 299 roughly the same results as on flat samples.⁴¹
18
19
20

21 300 2.1.2. Exogenous topography: micro/nanostructure through additive 22 23 301 strategies on metals 24 25

26 302 Additive strategies give access to more diverse topography geometries. By incorporating various
27
28
29 303 micro or nano objects to the metallic surface, some research teams developed antibiofouling
30
31
32
33 304 surfaces with more complex topographies. These are referred to as exogenous topographies.
34
35

36 305 2.1.2.1. Electro-deposition. 37 38

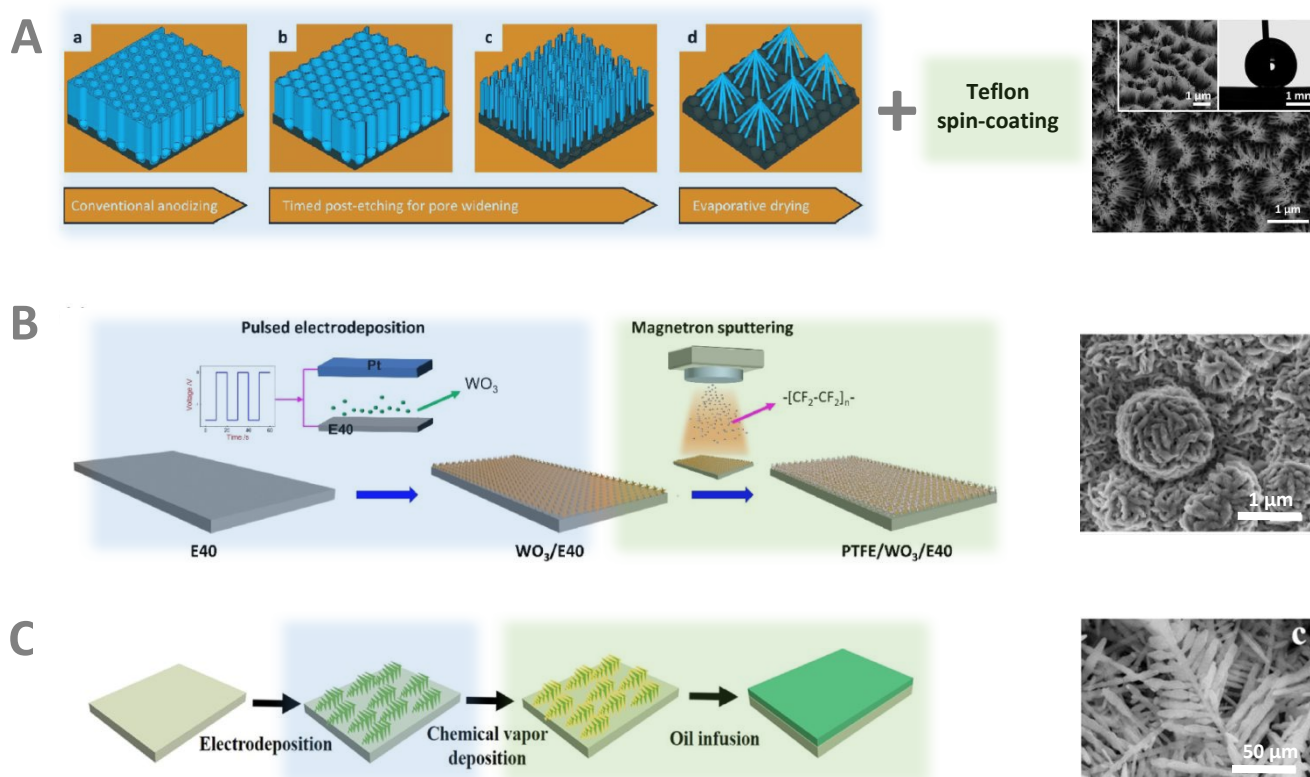
39 306 By using a metallic substrate as an electrode, electro-deposition of diverse conducting substances
40
41
42
43 307 can be achieved. For instance, using copper foil as an electrode exposed to a phosphate containing
44
45
46 308 electrolyte, Bao *et al*/produced microflower-like structures composed of copper and phosphate ions
47
48
49 309 complexes. Although no biological anti-fouling experiments were conducted, a superhydrophobic
50
51
52
53 310 self-cleaning and anti-corrosion surface was obtained after dodecylamine coating.⁴² Inspired by
54
55
56
57
58
59
60

1
2
3
4 311 similar research,^{43,44} the team of Chang-Hwan Choi chose aluminium foil to be anodized in an
5
6
7 312 oxalic acid solution to obtain a nanoporous structure that was thinned down with phosphoric acid
8
9
10 313 treatment, resulting in disconnected nanopillars. After evaporation under controlled conditions,
11
12
13 314 clusters of nanopillars assembled into conical nanostructures. A TeflonTM coating was finally
14
15
16
17 315 applied to obtain a superhydrophobic surface (Figure 6A) which was submitted to biofouling tests
18
19
20 316 against *E. coli* and *S. aureus* in static and dynamic conditions.⁴⁵ Up to 4-log reductions were
21
22
23 317 obtained upon bacterial adhesion testing for conical pillars covered with TeflonTM only, confirming
24
25
26
27 318 the synergy between the nanotopography and surface chemistry. A more recent study used
28
29
30 319 Na₂WO₄·2H₂O electrolyte to create flower-like nanosheets through electro deposition onto
31
32
33 320 polished E40 steel. The treatment was followed by high vacuum sputtering of PTFE and resulted
34
35
36
37 321 in a superhydrophobic micro/nano structured PTFE/WO₃ coated E40 steel substrate (Figure 6B)
38
39
40 322 with anti-pollution, anti-icing and antibiofouling properties (also obtained on Cu, Mg and Ti
41
42
43 323 alloys). *Shewanella algae* adhesion was completely avoided over 14 days immersion in the bacterial
44
45
46
47 324 suspension, while raw E40 steel and PTFE coated steel were covered with bacteria. The
48
49
50 325 superhydrophobicity and electrostatic repulsion arising from the synergistic combination of
51
52
53 326 micro/nano-structure and PTFE coating are believed to explain such results.⁴⁶ However, the WO₃

1
2
3
4 327 coated-only steel was not part of the antifouling characterized samples. It could have helped to
5
6
7 328 better distinguishing contributions of micro/nano-structure *vs* chemical surface composition for
8
9
10 329 explaining antibiofouling results. Ouyang and co-workers grew dendritic Ag micro/nanostructures
11
12
13 330 through Ag electro-deposition onto Titanium substrates, followed by dodecanethiol vapor
14
15
16
17 331 deposition and dimethyl silicone oil infusion to produce a Slippery Liquid-Infused Porous Surface
18
19
20 332 (SLIPS) (Figure 6C). A reduction by 4 orders of magnitude of diatom *Navicula minima* and green
21
22
23
24 333 algae *Chlorella vulgaris* was achieved upon 14 days of incubation.⁴⁷
25
26
27
28
29
30
31
32
33
34
35
36
37
38
39
40
41
42
43
44
45
46
47
48
49
50
51
52
53
54
55
56
57
58
59
60

334

335 *Figure 6: Combined approaches using electro-deposition based methods for topography design. A:*
 336 *clusters of nanopillars assembled into conical nanostructures obtained from anodization of aluminum foil*
 337 *and phosphoric acid treatment with a Teflon™ top layer (adapted with permission from reference ⁴⁵.*
 338 *Copyright 2017 American Chemical Society). B: flower-like nanosheets produced with Na₂WO₄·2H₂O*
 339 *electrolyte on polished steel, covered with PTFE sputtered layer (adapted with permission from reference*
 340 *⁴⁶, Copyright 2022 Elsevier). C: liquid-infused superhydrophobic dendritic silver matrix on titanium*
 341 *(adapted with permission from reference ⁴⁷, Copyright 2019 Elsevier). Blue and green overlay indicate*
 342 *topography and chemistry modifications, respectively.*



343 Beyond electrolyte-based electro-deposition treatments, it is also possible to coat conductive

344 polymers and obtain an antibiofouling effect. Stainless steel surfaces were turned

345 superhydrophobic by electrodeposition of hydrophobic and conducting poly(3,4-

346 ethylenedioxythiophene) (PEDOT) under the form of nanofibers.⁴⁸ Bacterial adhesion and biofilm

1
2
3
4 347 growth were investigated against *Pseudomonas aeruginosa* PAO1 and *Listeria monocytogenes* CIP
5
6
7 348 103574 (commonly found in medical facilities and food industry environments). The smallest value
8
9
10 349 of deposition charge (1 mC.cm⁻², without nanofibers), did not reduce the bioadhesion. On the
11
12
13 350 contrary, higher deposition charge (35 mC.cm⁻²), producing expanding vertical nanofibers, reduced
14
15
16
17 351 the bioadhesion by 3-4 log. This result confirmed that the superhydrophobic chemistry alone was
18
19
20 352 not enough to reduce the bacterial bioadhesion. A prominent surface topography was necessary to
21
22
23 353 achieve bacterial adhesion reduction. Biofilm growth was also performed and biofilm biovolume
24
25
26
27 354 were measured. The same conclusions arised on the importance of surface topography to limit
28
29
30 355 biofilm development.

34 356 **2.1.2.2. Other methods**

35
36
37 357 Leaving aside electro-deposition, the next three articles use different exogenous methods to create
38
39
40 358 topography. The first approach relies on the production of layered double hydroxide (LDH) films.
41
42
43 359 Aluminium alloys were coated with lithium-aluminium (Li-Al) LDH films. This is known as
44
45
46
47 360 hydrotalcite preparation. The samples were functionalized with 4-amino-2-((hydrazine methylene)
48
49
50 361 amino)-4-oxobutanoic acid (AOA) and 1*H*,1*H*,2*H*,2*H*-perfluorooctyltriethoxysilane (PFOTES).
51
52
53
54 362 This method produced films with hydrophobicity, antibiofouling and anti-corrosion properties.⁴⁹
55
56
57
58
59
60

1
2
3
4 363 SEM analysis showed a nest-like rough structure for these films with vertically-grown crosslinked
5
6
7 364 nanoplates. These films showed good anti-adhesive properties towards *E. coli*, *Bacillus subtilis* and
8
9
10 365 sulfate reducing bacteria, with repellency over 96% for each species. Antibacterial activity against
11
12
13 366 Gram-positive, Gram-negative and anaerobic bacteria is provided by the guanadino group of the
14
15
16
17 367 AOA. Combined with the surface roughness and hydrophobicity, this leads to surfaces with high
18
19
20 368 antibiofouling capacities. Using atmospheric pressure plasma spraying (APPS), the liquid
21
22
23 369 precursor hexamethydisiloxane was deposited onto foodgrade stainless steel. Process parameters
24
25
26
27 370 were studied in a first paper which revealed the influence of the precursor flow on the surface
28
29
30 371 roughness and morphology of the resulting coated surface (denoted as PL).³⁷ This refers to the *Step*
31
32
33 372 *1&2 Simultaneous topography and chemistry* approach described on Figure 2. The particular
34
35
36
37 373 chemical surface composition, combined with the random nanostructures revealed by atomic force
38
39
40 374 microscopy (AFM), led to a strong reduction of fouling upon two consecutive runs in a pilot
41
42
43
44 375 pasteurizer. A second study was conducted to compare this PL sample with lotus-like (LL) and
45
46
47 376 SLIPS samples that were described earlier in the previous *endogenous* section. Upon the fouling
48
49
50 377 test in the pasteurizer, LL and SLIPS surfaces failed to overcome the durability of PL surfaces over
51
52
53
54 378 the two consecutive runs.³⁸ Different bacterial strains were tested on PL samples only and
55
56
57
58
59
60

1
2
3
4 379 compared to bare stainless steel surface: a very mild reduction of *S. aureus* adhesion was observed,
5
6
7 380 but a strong reduction of bacterial adhesion for rod-shaped bacteria was obtained: 58% and 80%
8
9
10 381 for *L. monocytogenes* and *Salmonella enterica* respectively. The round-shaped bacteria are able to
11
12
13 382 penetrate into the microspaces of the grain structures of the PL surface, while rod-shaped bacteria
14
15
16
17 383 cannot, and thus have less anchoring spots, leading to reduced adhesion. However, authors did not
18
19
20 384 discuss the viable or dead state of the adhered bacteria that usually allow for further understanding
21
22
23
24 385 of the anti-adhesion and/or contact bactericidal effect.

25
26
27
28 386 Finally, Selim and co-workers used alumina or zinc nanorods associated with PDMS on steel in
29
30
31 387 order to fight against marine fouling. In a first study, graphene oxide-alumina nanorod hybrid
32
33
34 388 sheets were enhanced with exfoliated PDMS chains. The optimal amount of 1 wt% nanofiller
35
36
37
38 389 ensured the best dispersion of the nanoparticles. The resulting coating exhibited
39
40
41 390 superhydrophobicity and fouling resistance. After 28 days *in vitro* exposure to *Micrococcus sp.*
42
43
44 391 (Gram-positive), *Pseudomonas putida* (Gram-negative) or *Aspergillus niger* (fungus), a sharp
45
46
47
48 392 reduction of cell viability was observed. Fouling resistance was also confirmed with a three-month
49
50
51 393 field assay in marine waters.⁵⁰ In another study, zinc oxide nanorods were embedded in a PDMS
52
53
54
55 394 matrix to produce a similar superhydrophobic coating on steel. The same bacteria and fungus were

1
2
3 395 used for fouling resistance tests and, again, an optimized amount of nanofiller was detected at 0.5%
4
5
6
7 396 above and below which the properties were lost. A 6-month field trial assay in natural seawater
8
9
10 397 confirmed the *in vitro* tests. In both of these studies, the micro/nano-roughness combined to low
11
12
13 398 energy surface chemistry is called to explain the results.⁵¹
14
15
16

17 399 **2.2. Glass and silicon substrates**

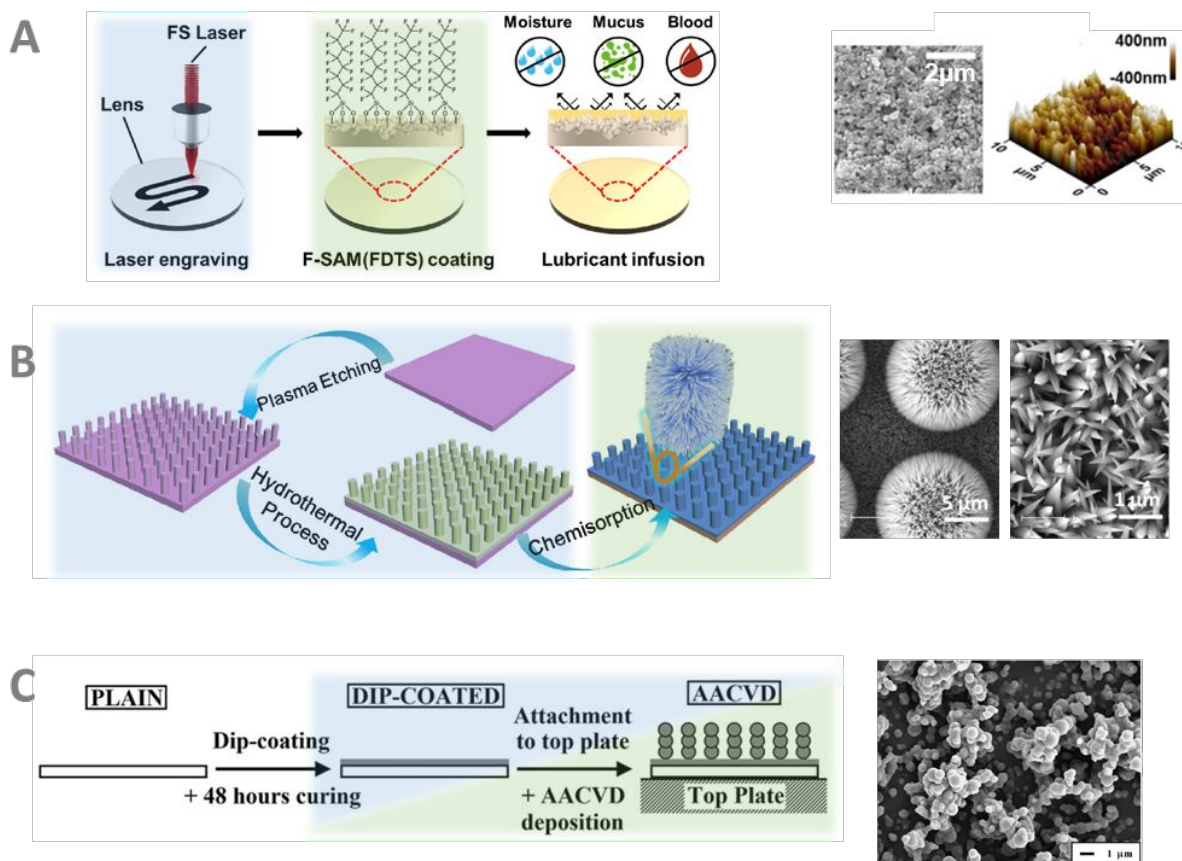
18
19
20 400 Regarding glass and silicon substrates, fewer articles dealing with combined topography and
21
22
23 401 chemistry approaches were encountered. The first one uses endogenous topography, produced
24
25
26 402 through laser patterning, while the second one uses both endogenous (reactive ion etching) and
27
28
29
30 403 exogenous topography with addition of another material (crystal seeding). All the others use
31
32
33 404 different exogenous topographies.
34
35
36
37

38 405 Lee *et al* addressed biofouling on endoscope lenses. In order to prevent bacterial infection and
39
40
41 406 fogging while achieving high mechanical durability, the lens was provided with a lubricant-infused
42
43
44 407 directly engraved nano/micro-structured surface (LIDENS).⁵² Femtosecond laser patterning was
45
46
47 408 first applied to the devices to obtain nanostructured surfaces. A coating of fluorinated self-assembly
48
49
50
51 409 monolayer was then added before infusion of the perfluorocarbon-based lubricant whose affinity
52
53
54 410 with the surface is increased with the fluorocarbon chains (see Figure 7A). The LIDENS coating
55
56
57
58
59
60

1
2
3
4 411 showed very good anti-adhesive effects towards blood which rolled off the surface without leaving
5
6
7 412 any trace. Fluorescent microscopy also demonstrated low adhesion towards albumin and
8
9
10 413 fibrinogen. In addition, tape-peeling and linear abrasion tests confirmed the robustness of the
11
12
13 414 LIDENS coating.

14
15
16
17 415 The next approach engraved the raw substrate to create micro-topography (endogenous), but also
18
19
20
21 416 used a new material to produce the nano-topography on top of it (exogenous). Inspired by the lotus-
22
23
24 417 leaf effect, silicon wafers were subjected to RIE to produce micro-cylinders. Zinc oxide crystal
25
26
27
28 418 seeds were then spincoated onto the microstructured surface allowing for the growth of Zinc salt
29
30
31 419 nanoneedles through low temperature hydrothermal reaction. Finally, a fluoroalkylsilane coating
32
33
34 420 was deposited by immersion in the silane solution, as depicted in Figure 7B. The resulting surface
35
36
37
38 421 exhibited superhydrophobicity with the Cassie-Baxter regime upon contact with liquid. A 99%
39
40
41 422 bacterial repellency was obtained even after 24h exposure to a bacterial suspension of *E. coli*,
42
43
44 423 compared to the flat untreated silicon wafer.⁵³ Moreover, the few bacteria that eventually adhered
45
46
47
48 424 onto the substrates were easily killed by the nanoneedles, as confirmed by their shrunken
49
50
51 425 morphologies (obtained by SEM) and non-viable state (by live/dead™ staining). The combination
52
53
54
55
56
57
58
59
60

of a topographical approach and relevant chemical surface treatment produced a synergistic
antibacterial solution.



428

429 *Figure 7: Combined approaches on glass and silicon-based substrates. A: endoscope lens with*
 430 *micro/nanostructure produced by femto-second laser ablation, covered with a fluorinated silane and*
 431 *infused with a perfluorocarbon-based lubricant (adapted from reference ⁵²). B: micro-cylinders produced*
 432 *by etching of silicon wafer and covered with zinc salts nanoneedles coated with a fluoroalkylsilane*
 433 *(adapted with permission from ⁵³, Copyright 2020 Elsevier). C: glass slides covered with a silicone*
 434 *elastomer and aerosol assisted chemical vapor deposition (adapted with permission from ⁵⁴, Copyright*
 435 *2011 Elsevier). Blue and green overlay indicate topography and chemistry modifications, respectively.*

436 In the following articles, exogenous materials are introduced to design both the topography and the
 437 chemistry.

1
2
3
4 438 Silane chemistry is of primary interest when silicon-based substrates are to be chemically modified.

5
6
7 439 Privett *et al* used nanostructured fluorinated silica colloids, fluoroalkoxysilane (heptadecafluoro-

8
9
10 440 1,1,2,2-tetrahydrodecyl)-trimethoxysilane (17FTMS) and methyltrimethoxysilane (MTMOS) to

11
12
13 441 develop superhydrophobic xerogel coatings which showed anti-adhesive properties towards *S.*

14
15
16 442 *aureus* and *P. aeruginosa*.⁵⁵ The particles showed both micro and nanoscale size. Acid-catalysed

17
18
19
20 443 hydrolysis and condensation was then performed to obtain 17FTMS/MTMOS films with or without

21
22
23 444 particles. The synergic combination of colloids and the fluorinated xerogel resulted in a

24
25
26
27 445 superhydrophobic surface. Soaking in water over 15 days did not affect the WCA, suggesting the

28
29
30 446 coatings were stable. These surfaces reduced bacterial adhesion by 99% for *S. aureus* and 98.2%

31
32
33 447 for *P. aeruginosa*.

34
35
36
37 448 In addition to liquid phase chemistry, vapor phase approaches were also used to tune silicon-based

38
39
40 449 substrates. Hence chemical vapor deposition techniques are able to bring both the topography and

41
42
43 450 the chemistry. In the first example, glass slides were covered with a silicone elastomer film through

44
45
46
47 451 dip-coating and subsequent aerosol assisted chemical vapor deposition (AACVD) of Sylgard® 184

48
49
50 452 silicon elastomer.⁵⁴ This process allowed for the formation of micro-scale random topographic

51
52
53
54 453 features, as described in Figure 7C. The bacterial adhesion on modified glass slides was evaluated

1
2
3
4 454 with *E. coli* and *S. aureus* through live/dead™ staining assay in 30 ml of 10⁷ colony forming unit
5
6
7 455 (CFU)/ml bacterial suspensions, maintained for 1 hour in static conditions. Non-adherent bacteria
8
9
10 456 were then removed and *BacLight*™ Bacterial Viability Staining kit was used to detect adhered
11
12
13 457 bacteria with fluorescence microscopy. The total amount of live and dead adhered bacteria was
14
15
16
17 458 drastically decreased on the modified glass slides, presumably because the aqueous bacterial
18
19
20 459 suspension is repelled by these surfaces.

21
22
23
24 460 An atmospheric plasma polymer coating was used to treat silicon wafers and produced a
25
26
27
28 461 microstructured topography while also imparting hydrophobic and superhydrophobic properties to
29
30
31 462 the surface, that prevent bacterial adhesion.⁵⁶ A mixture of docecyl acrylate and 1*H*,1*H*,2*H*,2*H*-
32
33
34 463 perfluorodecyl acrylate precursor was used. AFM imaging revealed a heterogeneous globular grain
35
36
37
38 464 structure. The wettability was studied with contact angle measurements to monitor the transition
39
40
41 465 from hydrophobic Wenzel regime to superhydrophobic Cassie-Baxter regime. The core of the
42
43
44
45 466 study lies in the fact that the authors performed statistical analysis to compare the influence of
46
47
48 467 different parameters on bacterial adhesion. These parameters were either related to the surface
49
50
51 468 (topography, chemistry, wettability) or to the bacterial medium in which the substrate was
52
53
54
55 469 incubated (bacteria species, culture, medium composition). The main result indicated that bacterial
56
57
58
59
60

1
2
3
4 470 colonization is by far predominantly influenced by culture conditions rather than surface properties.
5
6
7 471 This input is precious for researchers that tackle antibiofouling surface development since it
8
9
10 472 encourages them to use various medium conditions to assess precisely the antibiofouling
11
12
13 473 properties. The second result indicates that the superhydrophobic substrates were the more
14
15
16
17 474 effective at preventing bacterial adhesion, even after static or hydrodynamic long term culture. This
18
19
20 475 type of statistical analysis of the influence of culture conditions could be done for every type of
21
22
23
24 476 surface treatment that is developed to fight bacterial fouling.
25
26

27 477 **2.3. Polymer substrates**

28
29
30 478 As for a few of the metallic substrates, the following approaches dealing with polymeric substrates
31
32
33
34 479 can be separated into endogenous and exogenous topography. Molding techniques and plasma
35
36
37 480 treatments are highly represented in the former category, while co-polymers and inorganic
38
39
40
41 481 structures are used in the latter to design the topography.
42
43

44 482 **2.3.1. Endogenous topography: micro/nanostructure designed from** 45 46 483 **polymers**

47 48 49 484 **2.3.1.1. Molding**

50
51
52 485 Polymers are soft matter compared to metal and silicon-derived materials. Topographical features
53
54
55
56 486 can thus be easily obtained with simple thermal treatment of molding/templating processes, as it is
57
58

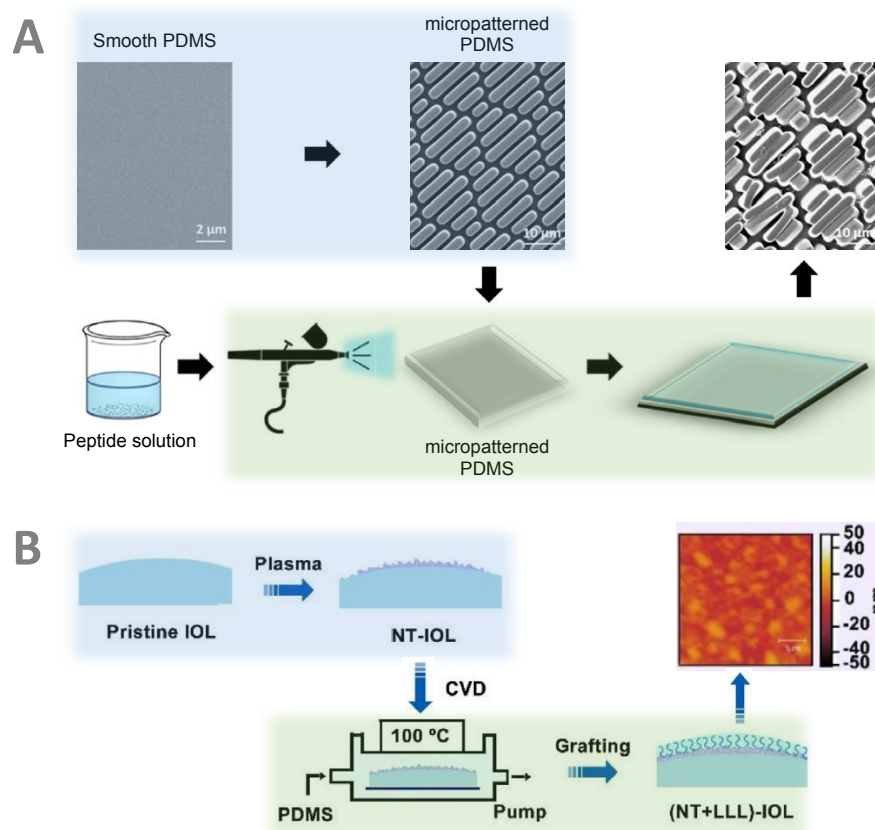
1
2
3
4 487 described in the next studies. Inspired by the pitcher plant, Ware and co-workers tuned the
5
6
7 488 topography of Teflon™ coated on polyethylene substrates with a simple thermal treatment at 160°C
8
9
10 489 to produce micro-wrinkles in which a silicon oil was then infused. The resulting superhydrophobic
11
12
13 490 surface demonstrated a 99% adhesion inhibition against *Pseudoalteromonas spp.* bacteria. The
14
15
16
17 491 inhibition was still above 76% after 2 weeks exposure to seawater. A complementary field test was
18
19
20 492 performed for 7 weeks in the ocean and the surface was only covered at 23% when reference
21
22
23 493 samples were fully covered with marine fouling.⁵⁷ The article also contains a brief overview of a
24
25
26
27 494 dozen studies related to lubricant infused surfaces that were tested against biological foulants such
28
29
30 495 as bacteria.

31
32
33
34 496 Dolid *et al* combined a shark-skin pattern on PDMS with a peptide-based coating to obtain
35
36
37
38 497 functional surfaces that repel bacteria.⁵⁸ A silicon wafer master produced by photolithography was
39
40
41 498 used to mold the structured shark-skin patterned surface, and a dopamine and peptide-based
42
43
44
45 499 mixture was then used to coat the PDMS substrates by a spraying technique, as depicted in Figure
46
47
48 500 8A. The water contact angle reached 119°. Upon testing against *E. coli* adhesion, it was shown that
49
50
51 501 the chemically and topographically modified surfaces reduced bacterial adhesion by 85% in
52
53
54
55 502 comparison to bare substrates. With *S. epidermidis*, adhesion reduction reached 72%. Dynamic

1
2
3
4 503 assays were also carried out with *E. coli* and demonstrated that no adhesion occurred on the peptide-
5
6
7 504 coated and patterned substrates.
8
9

10
11 505 **2.3.1.2. Plasma treatment**
12

13 506 Plasma treatment can easily and rapidly modify the topography of polymers. In the next studies,
14
15
16
17 507 different plasma treatments are used to modify the topography of polymer substrates. Oxygen
18
19
20 508 plasma treatment is a very common process and can easily modify polymers' topography. But other
21
22
23 509 gases are able to form plasma, and their combination with fluorinated carbon compounds lead to
24
25
26
27 510 topography modification as well as hydrophobization.
28
29
30
31
32
33
34
35
36
37
38
39
40
41
42
43
44
45
46
47
48
49
50
51
52
53
54
55
56
57
58
59
60



511
512 *Figure 8: Combined approach with endogenous topography design. A: shark-skin pattern on PDMS with a*
513 *peptide-based coating (adapted with permission from reference ⁵⁸, Copyright Elsevier 2020). B: intra-*
514 *ocular lens with nanotopography produced by oxygen plasma and covered with PDMS brushes to obtain*
515 *a liquid-like surface (adapted with permission from reference ⁵⁹, Copyright Elsevier 2021). Blue and green*
516 *overlay indicate topography and chemistry modifications, respectively.*

517 In order to prevent posterior capsule opacification (PCO) after cataract surgery, caused by adhesion
518 of residual lens epithelial cells, researchers from Sun Yat-sen University imparted an intraocular
519 lens (IOL) with nanotopography combined with PDMS brushes impregnated with silicon oil.⁵⁹ An
520 oxygen plasma treatment on the hydrophobic acrylic IOL formed the nanotopography. The PDMS
521 brushes were then tethered through a CVD system with the silicon oil (Figure 8B). The free end of
522 the grafted polymer chain formed a liquid-like coating. AFM confirmed the superior roughness of

1
2
3
4 523 the prepared surfaces. The enhanced IOL was also as transparent and mechanically resistant as the
5
6
7 524 pristine IOL. Anti-bioadhesion and cell viability experiments as well as animal testing
8
9
10 525 complemented with statistical analysis were performed. Bioadhesion is reduced the most when
11
12
13 526 topography and the chemical liquid-like layer are used simultaneously. The same outcome was
14
15
16
17 527 confirmed for cell viability. After 60 days of *in vivo* experiments, the enhanced IOL demonstrated
18
19
20 528 excellent biocompatibility and anti-PCO effect.

21
22
23
24 529 Oxygen plasma micro/nano-texturation was also performed on poly(methyl-methacrylate)
25
26
27
28 530 (PMMA) transparent sheets. Combined with metal-sputtering and/or hydrophobic film deposition,
29
30
31 531 antibiofouling and antimicrobial properties were obtained.⁶⁰ Two different hydrophobic coatings
32
33
34 532 were finally used: octafluorocyclobutane (C₄F₈) that was deposited through plasma again, and
35
36
37
38 533 perfluorooctyltrichlorosilane (pFOTS) through vapor deposition after oxygen plasma activation.
39
40
41 534 For this review, the focus here covers only the textured PMMA sheets modified with hydrophobic
42
43
44
45 535 coatings only (no metals). These samples were immersed in a bacterial suspension of unicellular
46
47
48 536 Gram-negative cyanobacteria *Synechococcus sp.* for 72 hours in order to study bacterial adhesion.
49
50
51 537 A resulting coverage of less than 1.5% was detected, suggesting efficient anti-adhesive properties.
52
53
54
55 538 However, the author did not discuss the potential synergistic effect of the micro/nano-texture and
56
57
58
59
60

1
2
3
4 539 hydrophobic coatings. Experiments with hydrophobic coatings on PMMA without the micro/nano
5
6
7 540 texture would have helped on this matter.
8
9

10
11 541 Argon and Argon/CF₄ plasmas were used to modify polycarbonate substrates. The Argon/CF₄
12
13
14 542 treatment imparted both topography and specific surface chemistry that reduced bacterial and
15
16
17 543 microalgae adhesion.⁶¹ AFM measurements revealed that Ar plasma alone was not able to modify
18
19
20
21 544 the polycarbonate substrates topography. Only Ar/CF₄ plasmas increased the roughness
22
23
24 545 significantly. Bioadhesion tests were performed in flow-cells with bacterial (two Gram negative
25
26
27
28 546 marine bacteria, *Paracoccus sp.* 4M6 and *Pseudoalteromonas sp.* 5M6) and diatom (two axenic
29
30
31 547 microalgae strains, *Cylindrotheca closterium* AC-170 and *Porphyridium purpureum* AC-122)
32
33
34 548 cultures. Bacteria were exposed 2 h to the surface while 24 h exposure with 12 h-12 h light-dark
35
36
37
38 549 cycle was carried out with microalgae. The main outcome is that only the Ar/CF₄ treated
39
40
41 550 polycarbonate with higher content of CF₄ managed to reduce the adhesion of the tested micro-
42
43
44 551 organisms (65% to 90% reductions). The authors claim the combination of surface chemistry and
45
46
47
48 552 nano-topography explains such a result. The stability of the modified substrates was also evaluated
49
50
51 553 with contact angle measurements after 1 hour-treatment with 2.6% bleach, and no effect was
52
53
54
55 554 detected.
56
57
58
59
60

1
2
3 555 **2.3.2. Exogenous topography: micro/nanostructure through additive**
4
5 556 **strategies on polymers**
6
7

8 557 Polymer surface topography can also be modified by the deposition of a polymer of different
9
10
11 558 nature, but inorganic structures are also used as exogenous material to tune the topography.
12
13

14
15
16 559 Inspired by frog skin, this approach consisted in coating a PDMS layer with a block copolymer of
17

18
19 560 polystyrene (PS) and polylactic acid (PLA). Upon an hydrolytic treatment, the PLA blocks were
20

21
22 561 degraded generating microwrinkled surfaces due to the kinetic release of local strains along the
23

24
25
26 562 multilayer composite. In addition, the volumes freed from PLA blocks formed a nanoporous
27

28
29 563 structure with co-continuous nanochannels. Finally, a silicon oil was infused into the porous
30

31
32
33 564 structure thanks to capillary forces in order to produce a wrinkled SLIPS.⁶² Antibiofouling
34

35
36 565 properties were assessed against the green algae species *Chlorella* sp. DT through cell coverage
37

38
39
40 566 analysis after immersion in a suspension in static conditions for 7 days. Further evaluation was
41

42
43 567 performed in fresh seawater for 7 days with blue-green algae species (*Arthrospira platensis* and
44

45
46 568 *Synechococcus lividus*), seawater algae species (*Isochrysis galbana*, *Tetraselmis ehui*) and
47

48
49 569 filamental cyanobacteria under different culture conditions that mimick the natural environments
50

51
52
53 570 of these microorganisms. Without the silicon oil (topographical approach only), in static condition
54

1
2
3
4 571 assays, antibiofouling performance was slightly improved when increasing wrinkle interspaces.
5
6

7 572 The author explains this tendency by indicating that the 15 μm green algae has less attachment
8
9

10 573 points with increasing the wrinkle wavelength. However, performance dramatically improved after
11
12

13 574 silicon oil infusion, especially for the largest (75 μm) wrinkle wavelength. This illustrates the
14
15

16
17 575 beneficial effects of the combination of both topography and chemistry for antibiofouling
18
19

20 576 performance. Testing in dynamic conditions lead to similar results. The authors also tested an oil-
21
22

23 577 infused substrate without the wrinkling structure (chemical approach only). Its performance was
24
25

26
27 578 lower than substrates with combined approaches. However, it appeared that the lubricant is hard to
28
29

30 579 retain in dynamic conditions. Finally, optical transparency, anti-icing and self-cleaning properties
31
32

33 580 were demonstrated for the wrinkled oil infused substrates, confirming their high potential for
34
35

36
37 581 sensors or optical devices in marine industry.
38
39
40

41 582 Another example of topography modification with added material relied on the growth of Nickel
42
43

44 583 hydroxide $\text{Ni}(\text{OH})_2$ onto a cotton fabric, followed by immersion in stearic acid solution and thermal
45
46

47
48 584 treatment to produce nickel stearate broccoli-like micro-structures. The modified cotton fabric was
49
50

51 585 turned superhydrophobic (160°), and suppressed bacterial growth of Gram-positive *S. aureus* and
52
53

54
55 586 Gram-negative *E. coli*, as well as fungal growth of *Candida albicans* even if the antibacterial
56
57
58
59
60

1
2
3
4 587 mechanism remains unclear (Ni^{2+} release is suggested to play a role).⁶³ Cotton fabric was also
5
6
7 588 modified with SiO_2 nanoparticles enhanced with photodynamic activity of chlorin e6 (Ce6) and
8
9
10 589 functionalized with perfluoroalkyl-silane as described in Figure 9A. The textile's antibiofouling
11
12
13 590 property was evaluated against suspensions of Gram-positive *S. aureus* and Gram-negative *E. coli*.
14
15
16
17 591 Immersion and spraying in the dark were the two methods of exposure to the microorganisms,
18
19
20 592 modelling waterborne and airborne bacterial contamination, respectively. The synergistic effect of
21
22
23 593 superhydrophobic coating with perfluoroalkyl-silane and air trapping by hierarchical
24
25
26
27 594 nanostructures was proposed as an explanation for the significant reduction of bacterial adhesion
28
29
30 595 (*ca.* 90%) for both strains in the immersion approach. Similar results were obtained for the spraying
31
32
33
34 596 approach. Remaining bacteria elimination was expected to be eradicated by the photodynamic
35
36
37 597 activity of Ce6 that generates reactive oxygen species (ROS) upon visible light illumination. The
38
39
40 598 modified cotton textiles demonstrated a clear 100% killing rate against both *S. aureus* and *E. coli*
41
42
43
44 599 after 45 min of light illumination. Finally, modified textile fibers were exposed to whole blood and
45
46
47 600 managed to entirely repel the complex medium upon roll-off experiments.⁶⁴
48
49
50
51
52
53
54
55
56
57
58
59
60

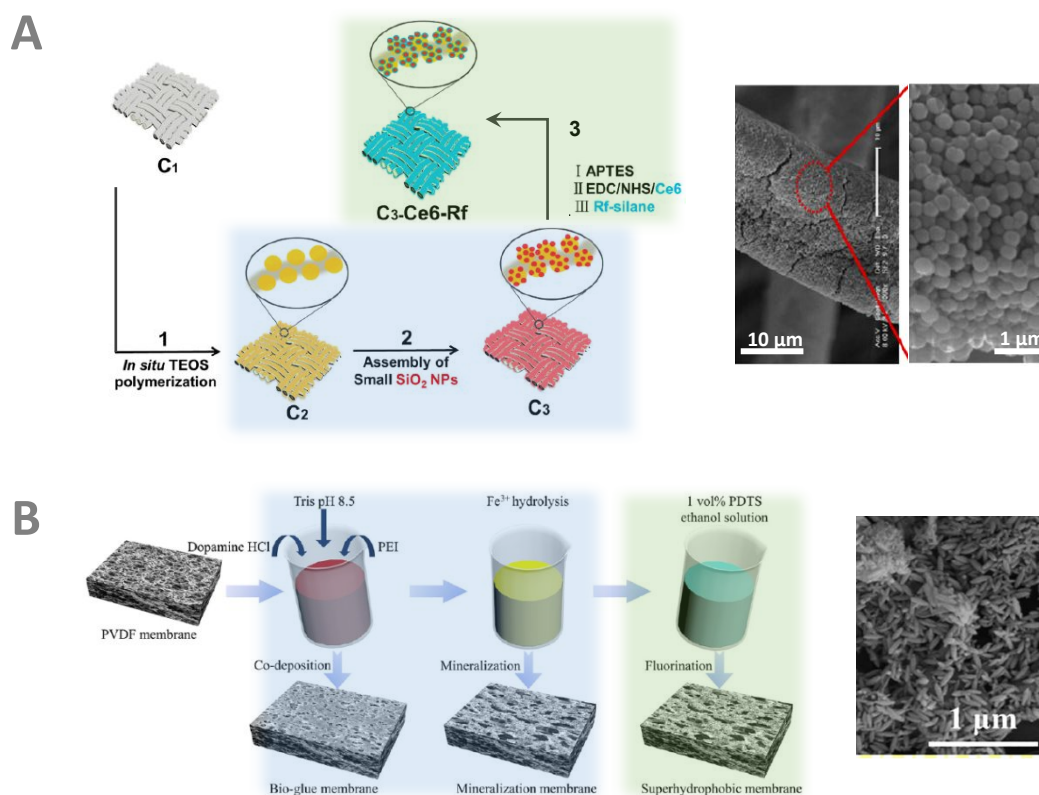


Figure 9: Combined approach for exogenous topography design. A: cotton fabric enhanced with SiO₂ nanoparticles further coated with chlorin e6 and perfluoroalkylsilane (adapted with permission with reference ⁶⁴, Copyright 2019 American Chemical Society). B: PVDF membrane treated with β-FeOOH nanorods embedded in a polymer matrix, covered with a perfluorosilane (adapted with permission from reference ⁶⁵, Copyright Elsevier). Blue and green overlay indicate topography and chemistry modifications, respectively.

The final article of this sub-chapter deals with a polyvinylidene fluoride (PVDF) membrane modified through mussel-inspired strategy: the co-deposition of polydopamine and polyethylenimine as biogluce to embed β-FeOOH nanorods. A final top layer chemistry of perfluorosilane was also used to further improve the superhydrophobic properties (see Figure

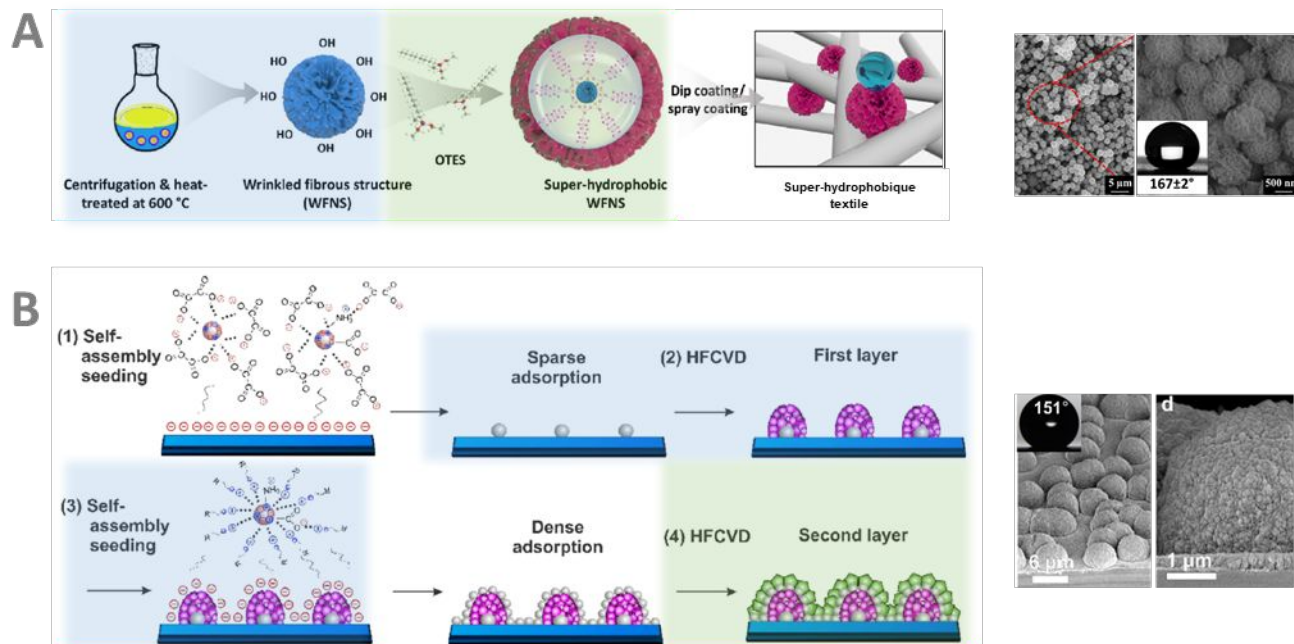
1
2
3 613 9B).⁶⁵ Roll off angles below 6° were measured. Moreover, thermal and mechanical resistance were
4
5
6
7 614 evaluated for an hour against ultrasonic treatment, or 85°C aqueous medium. Contact angles were
8
9
10 615 not affected at all. The performance of direct contact membrane distillation (DCMD) was
11
12
13 616 performed with the pristine and enhanced membranes. Model wastewaters were used: a mixture of
14
15
16
17 617 NaCl, CaCl₂ and NaHCO₃ or NaCl and sodium dodecyl sulfate. The superhydrophobic membrane
18
19
20 618 outperformed the pristine membrane in every case with delayed compromised flux and no salt
21
22
23 619 crystallization. Even after 60h long DCMD testing, the nanorods were still present and the
24
25
26
27 620 membrane still functional. According to the author, the clear contribution of both the structured
28
29
30 621 nanorods and the chemical fluor layer contributed to reach the Cassie-Baxter regime that prevents
31
32
33 622 membrane wetting and explains such results.

37 623 **2.4. Multi-substrate approaches**

38
39
40 624 In this last subchapter the focus is given to the research articles that offer a combined topography
41
42
43
44 625 and chemistry approach for antibiofouling surface modification that have been successfully applied
45
46
47 626 to substrates of different nature. Indeed, from an applicative engineer perspective, such approaches
48
49
50
51 627 are of great interest since they might be used in various industrial fields, regardless of the nature of
52
53
54
55
56
57
58
59
60

1
2
3
4 628 the materials to be protected. These approaches inherently fall into the exogenous topography
5
6
7 629 category.
8
9

10
11 630 A robust superhydrophobic coating was developed through the use of wrinkled fibrous nano silica
12
13
14 631 functionalized with octyltriethoxysilane (OTES), as depicted in Figure 10A. Various substrates
15
16
17 632 (PVDF, glass, aluminium foil, fabric and paper) were treated with the wrinkled fibrous nano silica
18
19
20
21 633 dispersions by spray (hard substrates) or dip coating (soft substrates). The superhydrophobicity
22
23
24 634 was confirmed by contact angle measurements with daily liquid products such as honey, milk,
25
26
27
28 635 coffee, yogurt and juice. The robustness of the coating was demonstrated through abrasion testing,
29
30
31 636 finger wiping, tape adhesion and bending as well as before and after exposition to harsh
32
33
34 637 environmental conditions (UV light, organic solvents and salts, high temperatures). Also,
35
36
37
38 638 preliminary antifungal properties were revealed after exposition of a modified fabric to fungal
39
40
41 639 species under favorable conditions. The combination of the hydrophobic properties with the surface
42
43
44 640 roughness of the coral-reef like structure (and inherent air gaps) prevented the adhesion of micro-
45
46
47
48 641 organisms and drastically reduced the availability of nutrient in the liquid phase close to the
49
50
51 642 surface.⁶⁶
52
53
54
55
56
57
58
59
60



643

644 *Figure 10: Multisubstrates combined chemical and topographical approaches. A: wrinkled nano silica*
 645 *fonctionnalized with octyltriethoxysilane deposited on textile, aluminium foil, glass, PVDF, fabric and*
 646 *paper (adapted with permission from reference ⁶⁶, Copyright 2020 Elsevier). B: hot filament chemical*
 647 *vapor deposition for micro and nano sized diamond hemispheres, covered with perfluorosilane (adapted*
 648 *with permission from reference ⁶⁷, Copyright 2020 American Chemical Society). Blue and green overlay*
 649 *indicate topography and chemistry modifications, respectively.*

650 Fang *et al*/developed SLIPS with a one-step alcohol-assisted femtosecond laser irradiation that is
 651 able to create porous micro/nanostructures on different substrates: stainless steel, nickel, glass and
 652 polymer.⁶⁸ Fluoroalkylsilane modification was then carried out to reach superhydrophobic and
 653 oleophilic surfaces. Indeed, this surface coating modified the WCA from 13° on porous stainless
 654 steel, up to 143°. After silicon oil infusion onto the hydrophobic surface, the adhesion properties
 655 were further modified, showing much lower adhesion to water droplets. This was demonstrated for

1
2
3
4 656 various solutions with different components and viscosity: water, milk, ink, egg white, and
5
6
7 657 especially blood, which all simply slip down the tilted SLIPS. The substrates were tested in the
8
9
10 658 presence of green algae, a common fouling specie in marine applications. It was shown that the
11
12
13 659 combination of laser-irradiated structure and silicon oil lubricant was essential for obtaining a good
14
15
16
17 660 antibiofouling performance after seven days exposure to the green algae.

18
19
20
21 661 An antibacterial, self-cleaning and antibiofouling coating was obtained on commercial titanium
22
23
24 662 alloys, silicon, quartz and ceramic substrates.⁶⁷ The bottom-up process based on hot filament
25
26
27
28 663 chemical vapor deposition (HFCVD) allowed for the modification of complex geometries and large
29
30
31 664 scale substrates. A pre-seeding of the substrates was performed with detonation nanodiamond,
32
33
34 665 followed by the HFCVD process that triggered the growth of diamond hemispheres. This procedure
35
36
37
38 666 was repeated one time to grow an additional, smaller, diamond structure onto the first one. Finally
39
40
41 667 the samples were chemically modified in liquid FDTs after an oxygen plasma treatment (see Figure
42
43
44 668 10B). Antibacterial activity was evaluated against *P. aeruginosa* (MCCC1A00099) and *E. coli*
45
46
47
48 669 (ATCC 25922) by using live/dead™ staining after 24 hours incubation. These tests confirmed the
49
50
51 670 crucial role of the structured diamond film with *ca.* 90% and 99% reduction in bacterial adhesion
52
53
54
55 671 compared to untreated substrates for *P. aeruginosa* and *E. coli*, respectively. In addition, two

1
2
3
4 672 biofouling tests with marine contaminants *C. vulgaris* (FACHB 44) and *Ulothrix speciosa* (FACHB
5
6
7 673 494) were conducted. Again, the structured and fluorinated samples demonstrated the best
8
9
10 674 antibiofouling results compared to untreated samples, but also compared to the samples modified
11
12
13 675 with either topography or chemistry alone. Thus it is the synergistic effect of topography and
14
15
16
17 676 surface chemistry that allows for such antibiofouling effect.

18
19
20
21 677 As a conclusion, in a vast majority, the combined topography and chemistry hydrophobic
22
23
24 678 approaches to produce antibiofouling surfaces lead to superhydrophobic wettability, often
25
26
27
28 679 achieving Cassie-Baxter regime. In most articles, this result is obtained only by combining
29
30
31 680 topography with a specific surface chemistry. The antibiofouling property thus arises from the
32
33
34 681 prevention adhesion mechanism cited in Figure 1. However, despite the various topography
35
36
37
38 682 designing techniques, the hydrophobic chemical entities employed are limited to either fluorine-
39
40
41 683 based polymers or silanes, alkyl chains or infused silicon or fluorine-based oils. The next chapter
42
43
44 684 will demonstrate how wide the hydrophilic chemical entities library is for antibiofouling surface
45
46
47
48 685 development with combined topography and chemistry approaches.

49
50
51
52 686 **3. Combined topography and hydrophilicity for multiple antibiofouling**
53
54
55 687 **mechanisms**
56
57
58
59
60

1
2
3
4 688 As explained in the introduction, superhydrophilic surfaces can also be used for antibiofouling
5
6
7 689 surface development. In this chapter we will focus on research articles where superwettability has
8
9
10 690 been achieved by combining topography and chemistry with the aim to repel biomolecules and
11
12
13 691 microorganisms. Many different techniques have been used to develop the functional topography
14
15
16
17 692 and deposit the chemistry of interest. All the approaches described in this chapter are detailed in
18
19
20 693 Table S3 of the Supporting information.

21
22
23
24 694 Superhydrophilic surfaces have been less explored for antibiofouling applications than
25
26
27
28 695 superhydrophobic one. This can explain why less common ground can be found in the literature
29
30
31 696 and why there is such a variety of solutions. In addition, as it can be seen in Figure 2, there is a
32
33
34 697 wide range of chemical approaches leading to hydrophilic antibiofouling surfaces. This can make
35
36
37
38 698 it challenging to find links between the various articles. However, as in the previous chapter
39
40
41 699 concerning hydrophobic approaches, three types of substrates have been studied: metals, glass and
42
43
44
45 700 polymers. This will be used to structure this part of the review, thus creating three sub-chapters.

48 701 **3.1. Metallic substrates**

49
50
51
52
53
54
55
56
57
58
59
60

1
2
3
4 702 Metallic substrates are not a common material used for hydrophilic-based approaches, oppositely
5
6
7 703 to hydrophobic strategies. However, these surfaces show very different characteristics,
8
9
10 704 demonstrating the diversity of hydrophilic strategies for antibiofouling studies on metals.

11
12
13
14 705 The first example of such surfaces are TiO₂ nanotubes coated with a Poly(ethylene) glycol (PEG)-
15
16
17 706 silane, which showed different activities against fibrinogen and *S. aureus* depending on the size of
18
19
20
21 707 the nanotubes. For this study, An and co-workers used potentiostatic anodization of Titanium to
22
23
24 708 create the nanotubular effect. Two dimensions were created: nanotubes of 20 and 80 nm diameter
25
26
27
28 709 (TN20 and TN80 respectively). This was followed by a reaction with a PEG-silane solution
29
30
31 710 allowing the nanotubes to achieve better hydrophilicity (see Figure 11B). Although TN80 was more
32
33
34 711 hydrophilic with a WCA of 19°, TN20 was the only surface which showed both low adhesion of
35
36
37
38 712 model foulant fibrinogen and low friction coefficient. *S. aureus* was used to test the bacterial
39
40
41 713 adhesion. Surprisingly, PEG-coated TN20 showed a high adhesion, similar to Ti and PEG-coated
42
43
44 714 Ti, whereas all the other substrates, including PEG-coated TN80, repelled the bacteria. It seems
45
46
47
48 715 that, depending on the size of the nanotubes, and therefore, on the available surface contact area,
49
50
51 716 the antibiofouling effect can be inhibited.⁶⁹

1
2
3
4 717 This has also been shown through the study of marine diatoms on zwitterion-coated structured
5
6
7 718 stainless steel substrates. Here, unlike the previous study where the topography of the initial
8
9
10 719 substrate was modified, an exogenous material was added to create the topography. Indeed, the
11
12
13 720 initial substrates were coated with aluminium through flame spray technique and micropatterned
14
15
16
17 721 with a shielding steel mesh. A layer of PDMS was then formed on the samples and allowed for
18
19
20 722 subsequent chemical functionalization with the zwitterionic molecule [2-(Methacryloyloxy)ethyl]-
21
22
23 723 dimethyl-(3-sulfopropyl)-ammonium hydroxide (pSB) through 3,4-dihydroxyphenylalanine
24
25
26
27 724 (DOPA) binding. Bovine Calf Serum proteins were used to simulate the conditioning layer
28
29
30 725 formation on the substrates. An antibiofouling activity was observed but was fully attributed to the
31
32
33 726 hydration layer brought by the pSB and the electrostatic interaction between bovine proteins and
34
35
36
37 727 dipole moment of the sulfobetaine groups. No influence of the topography was detected. The
38
39
40 728 antimicrobial effect of the substrates was studied with marine diatoms *Cylindrotheca closterium*
41
42
43
44 729 which were incubated with the samples presenting both chemical and topographical modifications,
45
46
47 730 in an artificial seawater-based medium. Confocal laser scanning microscopy showed no adhesion
48
49
50 731 to the protuberances. However, pSB modification of reference flat samples resulted in a lower
51
52
53
54 732 density of diatoms. It is thought that the increase of the specific surface area of the patterned
55
56
57
58
59
60

1
2
3
4 733 substrates is responsible for the higher adhesion of diatoms. A hypothesis that can be raised is that
5
6
7 734 the protuberances are too big in comparison to the size of the tested micro-organisms.⁷⁰
8
9
10
11 735 One last type of metallic surface that has shown promise in antibiofouling applications due to its
12
13
14 736 hydrophilicity is bioinspired self-cleaning mucus-like hierarchical ciliary bionic antifouling
15
16
17
18 737 surfaces (SMCAS). These complex surfaces made of polyamide microfibers covered with carbon
19
20
21 738 nanotubes (CNT) and poly(vinyl alcohol) (PVA) hydrogel particles, that mimic the skin of marine
22
23
24 739 species, were designed by Ren *et al* with electrostatic flocking technology and solution spray (see
25
26
27
28 740 Figure 11A) to impart the so-called camouflage effect to steel surfaces, making them hard to be
29
30
31 741 recognised by the various foulants. Marine bacteria *Marinobacter lipolyticus* SM19(T) and
32
33
34 742 microalgae *Nitzschia closterium f. minutissima* were used to evaluate anti-adhesion performance of
35
36
37
38 743 the SMCAS surface. After 24 hours of co-culture, SMCAS integrally suppressed the bacterial
39
40
41 744 adhesion, showing better results than model PVA/CNT hydrogel which reduced the bacterial
42
43
44
45 745 adhesion to 2.0×10^3 cells/cm against 5.6×10^5 cells/cm on silicon. The efficacy of SMCAS,
46
47
48 746 explained by enhanced water-retaining, was also shown upon microalgae contact for as long as 3
49
50
51 747 weeks. Concomitantly, microfibers swaying along with the flow of seawater contributed to remove
52
53
54
55 748 the adhered contaminants.⁷¹
56
57
58
59
60

749

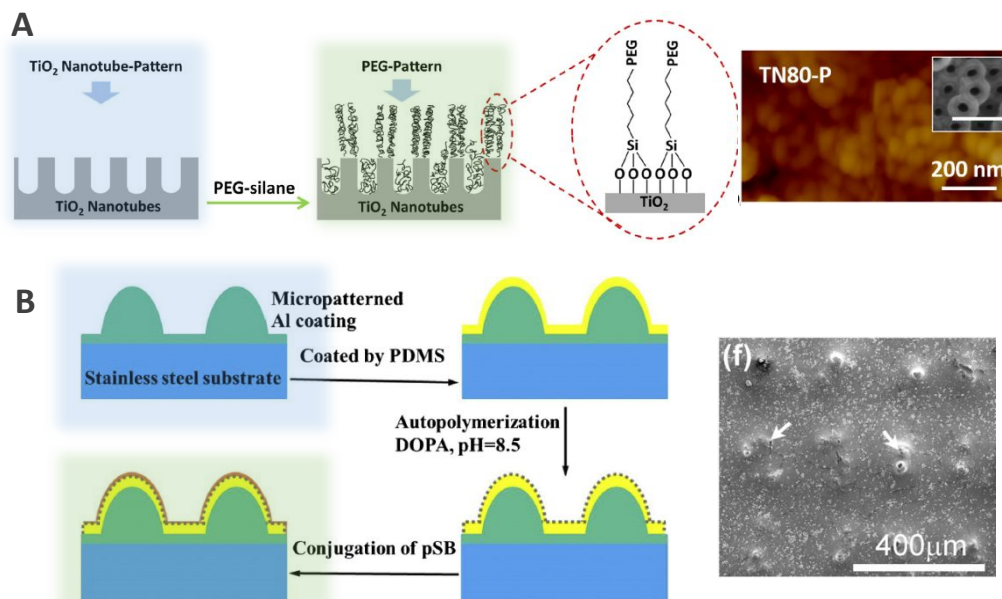


Figure 11: Antibiofouling strategies combining hydrophilic polymers and topography on metallic substrates. A: PEG silane on nanotubes (adapted with permission from reference ⁶⁹, Copyright 2019 Elsevier). B: Micropatterned Al coatings with zwitterion surface modification (adapted with permission from reference ⁷⁰, Copyright 2016 Elsevier). Blue and green overlay indicate topography and chemistry modifications, respectively.

3.2. Glass substrates

In this chapter, modified glass substrates with a hydrophilic antibiofouling activity will be described. The first three articles concern surfaces where endogenous topography has been created. The following articles use an exogenous material to tune the topography. They also show surface chemistry with a bactericidal effect on tested microorganisms, on top of the anti-adhesive effect caused by the hydrophilic coating on topography. This has enabled the creation of surfaces which

1
2
3
4 762 can kill bacteria as well as impede their adhesion. The following articles use an exogenous material
5
6
7 763 to tune the topography.
8
9
10
11 764 For example, nisin is an antimicrobial peptide with a hydrophilic end that has been combined to
12
13
14 765 microstructured glass to create efficient substrates against bacteria and diatoms. This study was
15
16
17
18 766 carried out by Lou and co-workers who began by structuring glass through ion etching before
19
20
21 767 functionalizing with nisin. This peptide binding protocol led to strong coatings which were stable
22
23
24 768 in sterile artificial sea water even after 10 days. The antibiofouling activity was assessed against
25
26
27
28 769 bacteria *Bacillus sp.* and diatoms *P. tricornutum*. The quadrangle-shaped microstructure alone
29
30
31 770 promoted bacterial fouling as the interspaces were bigger than the cells. However, with the nisin
32
33
34 771 immobilization, antibacterial effect was confirmed. Nevertheless, the synergistic effect of
35
36
37
38 772 microstructure and surface chemistry appeared hard to find for bacterial fouling. Against diatoms,
39
40
41 773 on the other hand, which are bigger than bacteria (10 μm vs 1-2 μm), the anti-adhesion effect of
42
43
44 774 the microstructure alone was stronger. With the nisin peptide treatment, an even better anti-
45
46
47
48 775 adhesion effect was detected, proving the synergistic effect of the combined approach against algal
49
50
51 776 foulants. Also, it was shown that an increased depth of the microstructure enhanced the anti-
52
53
54
55 777 adhesion effect of both untreated and nisin-treated glass microstructures against the diatoms.⁷²
56
57
58
59
60

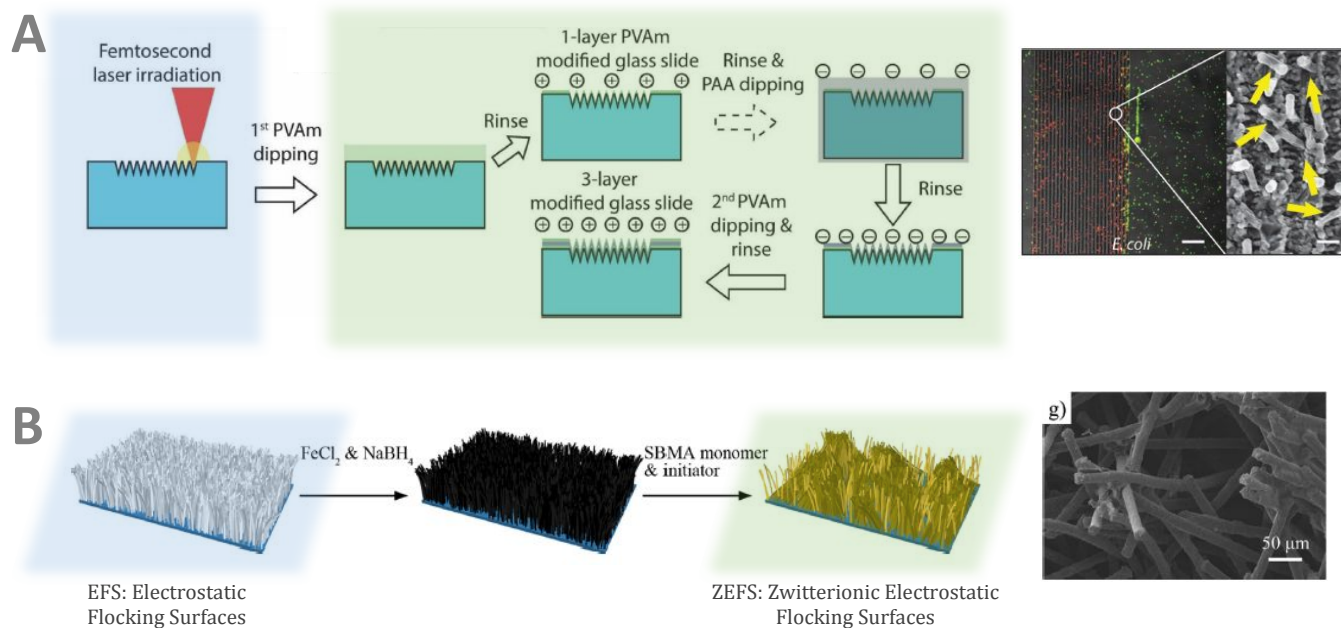
1
2
3
4 778 Polyacrylic acid (PAA) has also been used for its antibacterial effect. However, it has been shown
5
6
7 779 to have a gram-dependant efficiency. In a study by Chen *et al*, layer-by-layer deposition of
8
9
10 780 polyelectrolytes polyvinylamine (PVAm) and PAA was the chosen method for obtaining a
11
12
13 781 functional coating and femto-second laser pulsing was used to acquire micro and nano-patterned
14
15
16
17 782 borosilicate glass (see Figure 12B). When testing with *E. coli* K-12 and *S. aureus* 208, it was
18
19
20 783 confirmed that the positive charge surface enhanced bacterial collection. *E. coli* adhesion increased
21
22
23 784 faster than *S. aureus* owing to its higher outer-membrane charge. Live/Dead™ staining after a 4 h
24
25
26
27 785 incubation confirmed the bactericidal activity. It was suggested that the nanostructures contributed
28
29
30 786 more to the bactericidal effect than the microstructures. However, no damage was observed on
31
32
33 787 mammalian cells.⁷³

34
35
36
37 788 The same difference of adhesion depending on the type of bacteria was demonstrated with a film
38
39
40 789 of poly-(acrylic acid-co-(poly(ethylene glycol)diacrylate)) (poly(AAC-co-PEGDA)). Here, the
41
42
43
44 790 hydrogel was spin-coated onto functionalized cover slips and then treated with an argon plasma to
45
46
47 791 develop micro-sized wrinkles. The acrylic acid was efficiently bactericidal against both *S. aureus*
48
49
50 792 and *E. coli*, and the wrinkles contributed to lowering the amount of live microorganisms. However
51
52
53 793 the engineered surfaces were slightly more efficient on Gram-positive *S. aureus*.⁷⁴

1
2
3
4 794 Liu and co-workers produced a superhydrophilic layer of Poly(sulfobetaine methacrylate)
5
6
7 795 (PSBMA) by sub-surface initiated atomic transfer radical polymerization (SSI-ATRP) onto a glass
8
9
10 796 substrate. This technique allowed for the *simultaneous* tuning of both *topography and chemistry*
11
12
13 797 (as described in Figure 2). Micro-sized wrinkles were obtained, with size parameters depending on
14
15
16
17 798 the reaction time. A first study reveals the performance of the PSBMA structured surface against
18
19
20 799 marine environment conditions⁷⁵. Static antibiofouling was assessed with red algae *Porphyridium*
21
22
23 800 *sp.* and diatoms *Navicula sp.* for several hours. The resulting micro-organism densities were
24
25
26
27 801 reduced by two orders of magnitude for SSI-ATRP produced surfaces compared to blank surfaces.
28
29
30 802 Furthermore, on structured surfaces resulting densities were 4 to 6 times smaller than on
31
32
33 803 unstructured ones, indicating the beneficial synergistic effect of superhydrophilic surface chemistry
34
35
36
37 804 and microsized topography. Ocean field assays over 45 days were performed. According to the
38
39
40 805 author, the engineered surfaces better resisted the biofouling even if the available pictures seem
41
42
43
44 806 complicated to compare. The SSI-ATRP also improved the long-term stability of the polymer
45
46
47 807 layer.⁷⁵
48
49
50

51 808 The same team used the SSI-ATRP produced PSBMA layer in another study where the adhesion
52
53
54 809 of different types of foulants was investigated: macromolecules (BSA, lysozyme and fibrinogen),
55
56
57
58
59
60

1
2
3
4 810 bacteria (*E. coli* and *B. subtilis*) and diatoms (*Chaetoceros calcitrans*).⁷⁶ Here, a walnut-shell-like
5
6
7 811 microsized surface topography was obtained. It was shown that a 2 μm PSBMA layer prevents
8
9
10 812 macromolecular fouling, while a 5-10 μm thickness is more efficient against bacteria and diatoms.
11
12
13 813 After a longer reaction time (8 h instead of 1, 2 or 4), the regular walnut-shell-like structures
14
15
16
17 814 became irregular blocks and antibiofouling properties were lost.⁷⁶
18
19
20
21 815 PSBMA was also chosen to create zwitterionic electrostatic flocking surfaces (ZEFS). Unlike the
22
23
24 816 two formerly mentioned articles, here the topographical and chemical modifications were reached
25
26
27
28 817 through separate steps. The topography was first obtained by depositing nylon fibers onto glass
29
30
31 818 substrates by electrostatic flocking. A thin film of PSBMA was then wrapped around the
32
33
34 819 microfibers by radical polymerization catalyzed by Fe (see Figure 12A). It was demonstrated that
35
36
37
38 820 the diatoms *N. closterium f. minutissima* adhered very little to the fibers due to the low contact area
39
40
41 821 caused by their morphology. Further tests were carried out using common mussel species *Mytilus*
42
43
44
45 822 *edulis*, capable of choosing where to attach to the surface through exploration and thread secretion.
46
47
48 823 On a test board composed of glass, PDMS and ZEFS, the mussels avoided the zwitterionic coated
49
50
51 824 fibers, and preferentially stuck to glass.⁷⁷
52
53
54
55
56
57
58
59
60



825

826 *Figure 12: Fighting biofouling with hydrophilic coatings and topography on glass substrates. A: Layer-by-*
 827 *layer deposition of polyelectrolytes PVAm and PAA on nanopatterned borosilicate glass (adapted with*
 828 *permission from reference ⁷³, Copyright 2020 Elsevier). B: zwitterionic electrostatic floccing surface*
 829 *produced with PSBMA (adapted with permission from reference ⁷⁷, Copyright 2021 Elsevier). Blue and*
 830 *green overlay indicate topography and chemistry modifications, respectively.*

831 3.3. Polymer substrates

832 Polymer substrates are the most represented in the chapter focusing on hydrophilic combined
 833 approaches. In nearly two thirds of the research articles in this chapter, the initial material is a
 834 polymer. However, as well as the wide diversity found in the production of topography and the
 835 surface chemistry, there is also a large range of polymers themselves. These different polymers can
 836 have different physico-chemical properties and are therefore not all suited for the same
 837 applications. To facilitate reading, in this subchapter, the articles have not been organized

1
2
3
4 838 depending on the polymers, but rather on the application they were chosen for: marine industry,
5
6
7 839 water filtration, medical devices.
8
9

10 840 **3.3.1.1. Marine industry**

11
12 841 In this paragraph, the articles all aim to develop strategies for the marine industry where biofouling
13
14
15
16 842 can have a significant economic impact. Some teams use biomimetic materials, as sea species have
17
18
19 843 developed complex skin, shell or leaf surfaces to repel other, smaller organisms. Interestingly, they
20
21
22
23 844 all use PDMS as the initial substrate which is directly modified to obtain the desired topography.
24
25
26

27 845 In the first article, PDMS films were stretched and plasma-treated to obtain a wrinkled surface.
28
29

30 846 Silanization was then performed followed by surface-initiated atom transfer radical polymerization
31
32

33
34 847 (SI-ATRP) to produce poly(ethylene glycol)methacrylate (POEGMA) or poly(3-sulfopropyl-
35
36

37 848 methacrylate) potassium salt (PSPMA) brushes on the structured surface. The growth of the
38
39

40 849 polymer brushes did not have an impact on the structure. *Ulva* zoospores and microalgae *Chlorella*
41
42

43
44 850 were mixed in the same batch at different concentrations to evaluate the marine antibiofouling of
45
46

47 851 the different samples. In static conditions over 7 days, the PDMS wrinkled surface was able to
48
49

50 852 reduce the amount of adhered *Chlorella* more than *Ulva* since the zoospores are smaller than the
51
52

53
54 853 wrinkled surface size. The POEGMA and PSPMA layers on flat PDMS also showed reduced cell
55
56
57
58
59
60

1
2
3
4 854 densities. The combination of wrinkles and polymer brushes led to the smallest cell densities.
5
6
7 855 PSPMA-modified PDMS (both smooth and wrinkled) was more efficient than the surface modified
8
9
10 856 with POEGMA brushes against *Ulva* zoospores. However, there was no significant differences
11
12
13 857 between the two polymers against *Chlorella*. In dynamic conditions, very little biofouling from
14
15
16
17 858 *Chlorella* was detected: from ~240 cells/mm² on PDMS to under 20 cells/mm² on the modified
18
19
20 859 substrates. Finally, a sea water assay was performed for 2 months and clearly showed the superior
21
22
23
24 860 antibiofouling effect of SI-ATRP-modified wrinkled PDMS compared to wrinkled-only or bare
25
26
27 861 PDMS. Again, both polymer brushes showed similar antibiofouling effects.⁷⁸
28
29
30

31 862 Brzozowska's team took inspiration from marine decapod crab *Myomenippe hardwickii* and
32
33
34 863 replicated its surface composed of big and small features allowing it to repel species of various
35
36
37
38 864 sizes. To enhance the antibiofouling effect, the biomimicking structure was combined with surface
39
40
41 865 chemistry. Two strategies were carried out: modification with zwitterionic sulfobetaine polymer
42
43
44
45 866 brushes and layer-by-layer coating of poly(isobutylene-alt-maleic anhydride) and
46
47
48 867 polyethyleneimine (PEI) (Figure 13A). Tests were carried out with cyprids *Amphibalanus*
49
50
51 868 *amphitrite* and diatoms *Amphora coffeaeformis*. For both species, the lowest adhesion was
52
53
54
55 869 achieved with zwitterion brushes on patterned surfaces. This article also highlights the difference
56
57
58
59
60

1
2
3
4 870 between *in vitro* antibiofouling experiments and tests carried out in the field where hydrodynamics
5
6
7 871 have a non-negligible effect.⁷⁹
8
9

10
11 872 A similar approach consisted of mimicking the topography of algae *Laminaria japonica* by molding
12

13
14 873 PDMS. Layer-by-layer coatings were also applied. In this case, they were composed of sodium
15

16
17 874 alginate and (guanidine-hexamethylenediamine-Polyethyleneimine) (poly(GHPEI)) (Figure 13B).
18

19
20
21 875 Structuring and surface chemistry modification both led to better hydrophilicity in comparison to
22

23
24 876 bare PDMS. The most hydrophilic, with a WCA of 35°, was the (GHPEI-ALG)-coated structured
25

26
27
28 877 substrate. The prepared samples were tested against diatoms *N. closterium* and *P. tricornutum*.
29

30
31 878 Structured surfaces repelled diatoms better than smooth ones. However, the combination of
32

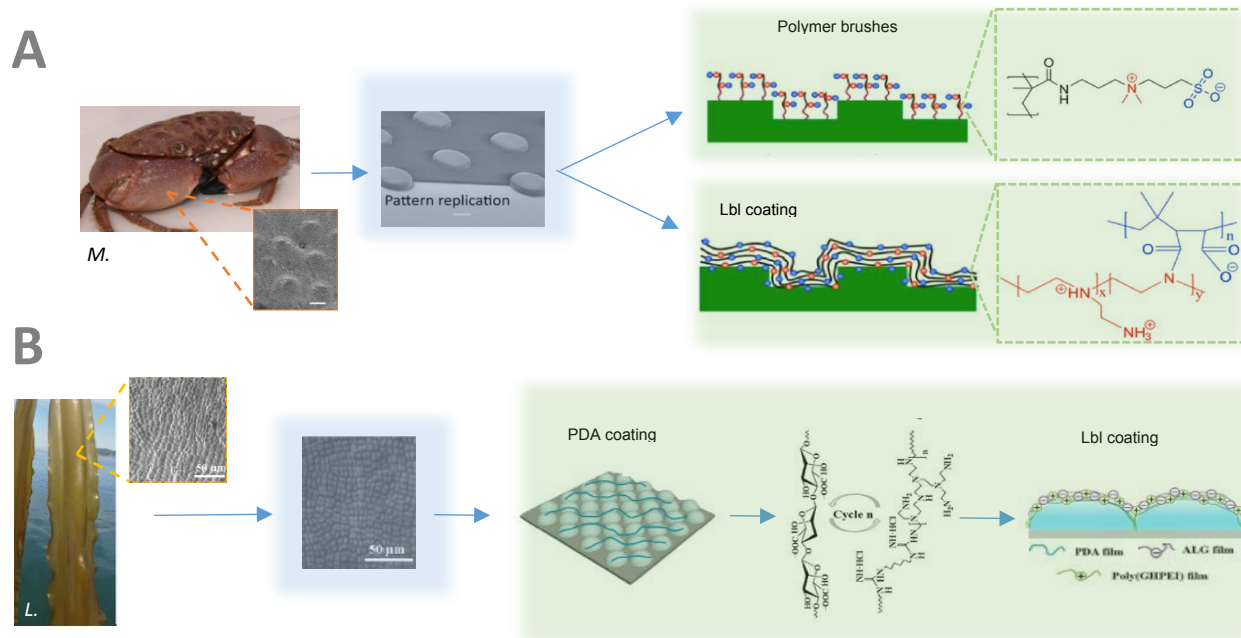
33
34 879 topography and chemistry gave the most effective surfaces, with a decrease in diatom density from
35

36
37
38 880 nearly 1200 diatoms/mm² on smooth PDMS to under 10 diatoms/mm² on the complex surface.
39

40
41 881 Over a period of 14 days, the developed material also inhibited diatom growth contrarily to other
42

43
44 882 materials. Antibacterial activity was also studied with *E. coli* and was evaluated to be roughly
45

46
47
48 883 96%.⁸⁰
49
50
51
52
53
54
55
56
57
58
59
60



884

885 *Figure 13: Bioinspired combinations of chemistry and topography on PDMS to fight marine biofouling. A:*
 886 *Biomimicking marine decapod crab M. hardwickii structure and modifying through polymer brushes or*
 887 *layer-by-layer coating (adapted with permission from reference ⁷⁹, Copyright 2014 American Chemical*
 888 *Society). B: Layer-by-layer coatings on molded PDMS inspired by algae L. japonica (adapted with*
 889 *permission from reference ⁸⁰, Copyright 2020 Elsevier). Blue and green overlay indicate topography and*
 890 *chemistry modifications, respectively.*

891 3.3.1.2. Water filtration

892 We have seen so far many different applications of antibiofouling surfaces but one important
 893 industry remains to be looked at: water filtration. Indeed, to avoid contamination of drinking water,
 894 it is vital that the polymer membranes that are used resist the formation of biofilm. Hydrophilic
 895 coatings have a true importance in this field to enhance the water separation. This is what will be
 896 studied in the next paragraph which is organised by type of polymer membrane used as the initial
 897 substrate.

1
2
3
4 898 The first one we will concentrate on is the polyamide (PA) membrane which has been chemically
5
6
7 899 and topographically modified by various teams, leading to efficient materials for water treatment
8
9
10 900 without biofilm formation.

11
12
13
14 901 Weinman and Husson for instance, structured PA membranes with nano lines and grooves by
15
16
17 902 thermal embossing, and coated them with poly(ethyleneglycol) diglycidyl ether (PEGDE) (Figure
18
19
20
21 903 14A). In comparison to pristine membranes, for which the flux was reduced by over 20% over a
22
23
24 904 period of 2 h, the patterned membranes did not have such a negative effect on the desired
25
26
27 905 application, with a maximum reduction of 8%. The PEGDE coating caused a slight flux reduction
28
29
30
31 906 on the patterned membranes but this impact did not increase with its concentration (5 or 15 wt%).

32
33
34 907 In all experiments the salt rejection remained close to the 95% specified by the manufacturer. To
35
36
37
38 908 test the antibiofouling capacity of these membranes, sodium alginate was used as a model foulant.

39
40
41 909 It was demonstrated, by quantifying the flux over time, that both the patterning and the chemical
42
43
44 910 coating decreased the fouling on the membranes. The combination of both surface hydrophilicity
45
46
47 911 and improved hydrodynamics induced by the lines and grooves, gave the best results.⁸¹

48
49
50
51
52 912 Choi's team, who had previously studied antibiofouling techniques based on cylindrical TiO₂
53
54
55 913 pillars on PA membranes,⁸² further improved their technique by upgrading the structuration of the
56
57

1
2
3
4 914 membranes to shark skin inspired topography, namely Sharklet™. They reached thin film composite
5
6
7 915 microstructured membranes using a series of steps including phase separation micromolding and
8
9
10 916 layered interfacial polymerization.^{83–85} The structure was then combined with coating of
11
12
13 917 hydrophilic tannic acid, deposited from the liquid-phase, giving the membrane an anti-adhesif
14
15
16
17 918 effect (Figure 14B).⁸⁵ Study of the modified membranes revealed NaCl rejection and permeability
18
19
20 919 towards water were very similar between uncoated and coated membranes. In fact, the water
21
22
23
24 920 permeance was slightly improved due to the hydrophilicity of the coatings. As with the nanopillar
25
26
27 921 arrays from their previous study,⁸² the sharkskin nanostructure coupled with a chemical coating of
28
29
30 922 tannic acid led to a decrease in *P. aeruginosa* attachment, shown qualitatively by live/dead™
31
32
33
34 923 imaging. In dynamic conditions, an isolated vortex is created by the Sharkskin protrusions,
35
36
37 924 decreasing furthermore the ability of *P. aeruginosa* to adhere to any surface⁸⁴. In their publication
38
39
40 925 from January 2022, Zhao *et al.* also used tannic acid on nanofiltration membranes for its
41
42
43
44 926 antibiofouling effect. They deposited it on a polyacrylonitrile membrane modified with
45
46
47 927 Glutaraldehyde (GA)-crosslinked PEI-SBMA to give it a microstructure which was tuned by
48
49
50 928 varying the concentrations of GA.⁸⁶
51
52
53
54
55
56
57
58
59
60

1
2
3
4 929 Another material with physico-chemical properties that allow the fabrication of membranes is
5
6
7 930 polysulfone (PSF). Various types of PSF membranes exist and have raised interest in the scientific
8
9
10 931 community.

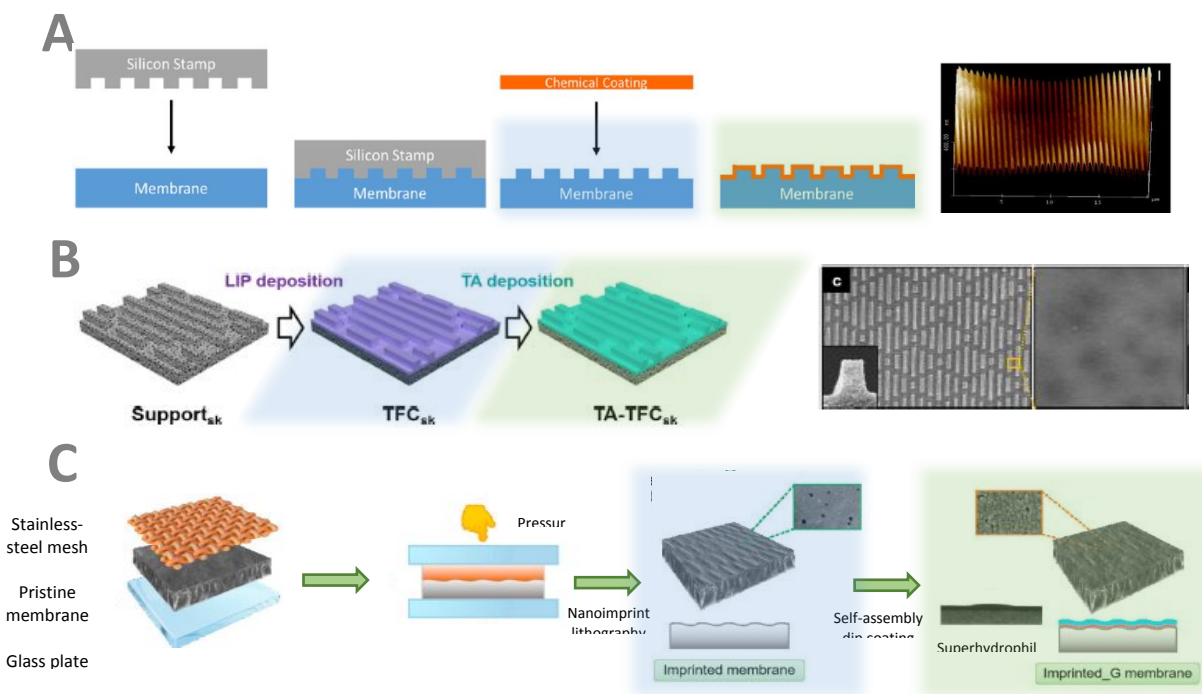
11
12
13 932 In a first study, a Polyethersulfone (PES) membrane was coated with a mixture of cellulose
14
15
16
17 933 nanofibrils (CNF) and PVA. This treatment imparted PES membranes with both nano-textured
18
19
20 934 roughness and charged surface chemistry. PVA was added to crosslink the film and improve its
21
22
23
24 935 adhesion to the substrate, decreasing the average roughness from around 30 μm to 10 μm .

25
26
27 936 According to the author, a smaller specific surface area is expected to better prevent molecule
28
29
30 937 adhesion. On the contrary of the wettability, which did not change, conserving the membrane's
31
32
33
34 938 efficiency; the surface charge was impacted by the coating: ζ -potential was reduced from -20 mV
35
36
37 939 to -40 mV around the plateau at pH 5, indicating a higher amount of negatively charged hydroxyl

38
39
40 940 and aldehyde groups. BSA adsorption on the coated membrane was evaluated using quartz crystal
41
42
43
44 941 microbalance with dissipation monitoring (QCM-D) and was shown to be very limited. It is
45
46
47 942 believed that the abundant hydrophilic groups of PVA/CNF layer suppress the interactions with
48
49
50 943 the protein. A biofilm study with *E. coli* revealed that the bacterial coverage was also almost
51
52
53
54 944 eliminated. In this case, the promising results can be explained by the combination of both surface

1
2
3
4 945 chemistry, which promotes electrostatic repulsion of bacteria and a bactericidal effect, and tuned
5
6
7 946 surface roughness, which reduces the specific surface area.⁸⁷
8
9
10 947 Lin and his team also chose to begin with PSF membranes, modifying them with a combination of
11
12
13 948 tannic acid (TA), PEI and (3-amino-1-propanesulfonic acid), otherwise known as taurine. Indeed,
14
15
16
17 949 these three molecules were co-deposited at the surface of the membrane, before interfacial
18
19
20 950 polymerization with trimesoyl-chloride. Turing striped structures were formed with 0.2% taurine
21
22
23
24 951 content during the interfacial polymerisation. Humic acid, sodium alginate and BSA were chosen
25
26
27 952 as model foulants. Flux recovery ratio was close to 98% against humic acid confirming excellent
28
29
30 953 antibiofouling effect. Sodium alginate and BSA tests gave slightly lower antibiofouling
31
32
33
34 954 performance (with a flux recovery ratio of 90% and 93% respectively), partly explained by higher
35
36
37 955 molecular weights. Here again, it is the combination of both chemistry and topography that led to
38
39
40 956 the best designed ultrafiltration membrane: the strong hydration layer arising from the zwitterionic
41
42
43
44 957 nature of taurine prevented the adsorption of model organic foulants, and meanwhile, the
45
46
47 958 hydrophilic striped surface allowed for a mild enhancement of water flux as a consequence of
48
49
50 959 increased specific surface area.⁸⁸ In a similar study from the same research team, interfacial
51
52
53
54 960 polymerization was combined to a sol-gel reaction in order to explore a new approach to limit

1
2
3
4 961 biofouling.⁸⁹ This led to controlled pore size and an increase in water permeability and selectivity
5
6
7 962 of the membrane. The surface was also enriched with hydroxyls that increased the hydrophilicity
8
9
10 963 and decreased the biofouling of BSA.
11
12
13 964 Finally, the last type of membrane that was found to be relevant for this review is the PVDF
14
15
16
17 965 membrane.
18
19
20
21
22
23
24
25
26
27
28
29
30
31
32
33
34
35
36
37
38
39
40
41
42
43
44
45
46
47
48
49
50
51
52
53
54
55
56
57
58
59
60



966

967 *Figure 14: Combining topography and hydrophilic coatings to combat biofouling on polymeric*
 968 *membranes for water treatment. A: Structured Polyamide (PA) membrane coated with*
 969 *Poly(ethyleneglycol)diglycidylether (PEGDE) (adapted with permission from reference ⁸¹, Copyright 2016*
 970 *Elsevier). B: PA membrane modified with Sharklet™ topography and coated with tannic acid (adapted*
 971 *with permission from reference ⁸⁵, Copyright 2021 Elsevier). C: Nanoimprint lithography and self-*
 972 *assembly dip-coating to modify PVDF membranes (adapted with permission from reference ⁹⁰, Copyright*
 973 *Elsevier 2020). Blue and green overlay indicate topography and chemistry modifications, respectively.*

974 For example, microporous PVDF membranes have been coated with poly(N-vinyl-pyrrolidone)
 975 (PVP) by initiated Chemical Vapor Deposition (iCVD). In this case, to increase the adhesion of the
 976 hydrophilic PVP onto the membrane, a prime layer of crosslinking agent poly (ethylene glycol
 977 diacrylate) (PEGDA) was deposited before coating with copolymer poly(VP-co-EGDA). Different
 978 ratios of crosslinking were tested and the effect on FTIR and WCA were analysed. The latter
 979 reached nearly 0°, as the water droplets got absorbed by the membrane in less than 3 s. It is thought

1
2
3
4 980 that this superwettability is only achieved by combining the two factors: the hydrophilicity of the
5
6
7 981 PVP coatings on the one hand, and on the other hand, the porous structure that allows the water
8
9
10 982 droplets to spread rapidly throughout the membrane. Antibiofouling was tested using model protein
11
12
13 983 BSA and fluorescently stained *E. coli*. The amount of BSA was reduced from 36 $\mu\text{g}/\text{cm}^2$ to under
14
15
16
17 984 2.2 $\mu\text{g}/\text{cm}^2$ upon coating the PVDF membrane. This quantity was slightly increased after durability
18
19
20 985 tests but still remained 90% lower than adsorption on pristine membranes. However, for these
21
22
23
24 986 estimations, only the apparent surface area was studied. It is thought that the internal pores have a
25
26
27 987 large surface area, thus decreasing furthermore the actual protein adsorption.⁹¹
28
29
30 988 Furthermore, in an article by Ma and co-workers, the PVDF substrates were enhanced by
31
32
33
34 989 modification of topography and grafting of nanoparticles decorated with hydrophilic chemical
35
36
37 990 functions. A micro scale surface pattern was formed through imprinting with a stainless steel mesh.
38
39
40 991 Further nano scale topography was achieved by adding an exogenous material. Indeed, the
41
42
43
44 992 imprinted membrane was dipped into a suspension of amine-terminated SiO_2 nanoparticles (see
45
46
47 993 Figure 14C). Simultaneously, amine functions that are not involved in the surface binding thus
48
49
50 994 represent the new surface chemistry of the membrane. It was noted that nanoparticle
51
52
53
54 995 functionalisation alone lead to high roughness, which was wiped out when combined with micro-

1
2
3 996 scale imprinting. Full wetting of water droplets observed during contact angle measurements
4
5
6
7 997 demonstrated the superhydrophilic nature of the modified membrane. Antibiofouling properties
8
9
10 998 were evaluated in both static conditions against bacteria suspensions (*Bacillus thuringiensis* and *E.*
11
12
13 999 *coli*) at 10^8 CFU/mL, and in dynamic conditions upon filtration tests with a practical mixed liquor
14
15
16
17 1000 sample in a full-scale aerobic membrane bioreactor. SEM analysis was used to detect the presence
18
19
20 1001 of bacteria. Fewer seemed to be detected on the modified membrane after rinsing, although no
21
22
23 1002 quantitative analysis was carried out. For the filtration tests, flux recovery measurements were
24
25
26
27 1003 performed to quantify the antibiofouling performance against the mixed liquor. The modified
28
29
30 1004 membrane offered a 45% higher flux recovery compared to pristine membranes, which is explained
31
32
33 1005 by the hydration layer arising from the superhydrophilicity, and the wave-like micro-structure that
34
35
36
37 1006 promotes turbulent flow, both reducing the adhesion of foulants to the membrane.⁹⁰
38
39

40 1007 **3.3.1.3. Medical devices**

41
42
43 1008 Polymers are also often used in the medical field as they have many advantages in comparison to
44
45
46
47 1009 other materials. In the case of medical devices, developing strategies to stop biofilm formation on
48
49
50 1010 the polymeric surface is even more critical as it can often lead to nosocomial infections.
51
52
53
54
55
56
57
58
59
60

1
2
3
4 1011 In this study, Park *et al* used a cellulose acetate (CA) solution which was drop-cast on a PDMS
5
6
7 1012 master mold resulting in a flexible CA nanoneedle array. After plasma treatment, an aqueous
8
9
10 1013 solution of 2-methacryloyloxyethyl phosphorylcholine (MPC) was spin-coated onto the array
11
12
13 1014 before drying in a convection oven. WCA proved the superhydrophilicity of the modified CA
14
15
16
17 1015 surface, with angles decreasing from 70° to 9°. Antibiofouling properties were evaluated against *E.*
18
19
20 1016 *coli* and *B. subtilis* suspensions in which they were incubated for 3 to 30 hours before live/dead™
21
22
23 1017 staining for fluorescence microscopy observations. Quantitative assays were also performed to
24
25
26
27 1018 confirm the antibacterial effect of the optically transparent substrates. The decrease of the density
28
29
30 1019 of detectable bacteria in fluorescence microscopy was mainly attributed to the chemical
31
32
33 1020 modification with MPC, while the live/dead™ staining assay confirmed that the nanoneedles were
34
35
36
37 1021 responsible for the bactericidal effect, by penetrating or stretching the bacterial membrane.⁹² The
38
39
40 1022 same team also modified poly(ethylene glycol) dimethacrylate (PEGDMA) nanoneedles which
41
42
43 1023 swell in wet conditions. Interestingly, they maintained their shape upon swelling, and similarly to
44
45
46
47 1024 the CA nanoneedles, the best antibiofouling effect was obtained for the sample that combined the
48
49
50 1025 chemical surface modification and the presence of nanoneedle topography. With the intrinsic
51
52
53 1026 antibiofouling properties of PEGMA, MPC-PEGMA nanoneedle hybrids proved to be tough

1
2
3
4 1027 antibiofouling surfaces as a local destruction of the topography or zwitterionic MPC coating was
5
6
7 1028 not sufficient to totally impede the antiadhesive properties of the substrates.⁹³
8
9
10
11 1029 Intraocular lenses have also been modified to avoid bacterial infection and minimize corneal cell
12
13
14 1030 attachment after cataract treatment. The lenses were altered by depositing a polymeric nanopillar
15
16
17
18 1031 array covered with ionic antibacterial polymer. The nanopillar array was produced by stamping a
19
20
21 1032 mix of polyurethane (PU) and Norland Optical Adhesive 63 polymer (PU/NOA63), onto a mold
22
23
24 1033 designed by photolithography. Then, iCVD was used to deposit a 50 nm thick layer of a copolymer
25
26
27
28 1034 of 4-vinylbenzyl chloride and 2-(dimethylamino)ethyl methacrylate. Thus, quaternary ammonium
29
30
31 1035 compounds (QACs) were introduced onto the surface of nanopillars. The antibacterial efficiency
32
33
34 1036 was measured against *S. aureus*. The nanopillar array alone demonstrated a 50% efficiency
35
36
37
38 1037 compared to flat PU/NOA63 polymer film, but it is only with the copolymer deposited on top that
39
40
41 1038 the antibacterial efficiency risen to almost 100%, confirming a profitable synergy between surface
42
43
44
45 1039 topography and chemistry. Upon adhesion, bacterial cells were captured in between the nanopillars,
46
47
48 1040 causing the latter to bend. The QACs available at the surface of the nanopillars are known to
49
50
51 1041 destabilize the bacterial membrane. When the nanopillars gradually restore their upright
52
53
54
55 1042 orientation, the bacteria slide down, and their membrane suffers deformation and then rupture.
56
57
58
59
60

1
2
3 1043 However, the engineered substrate showed biocompatibility for up to 7 days towards human
4
5
6
7 1044 corneal endothelial cells.⁹⁴
8
9

10 1045 **4. Conclusion & perspectives**

11
12
13
14

15 1046 As we have seen throughout this study, biofilm is a problem encountered in many different
16
17
18 1047 applications, ranging from medical devices to the marine industry. With antibioresistance and
19
20
21 1048 biocide resistance on the rise, and World Health Organization urging to take action, new
22
23
24
25 1049 antibacterial and antibiofouling strategies need to be developed. Concern is also arising over the
26
27
28 1050 toxicity of bactericidal nanoparticles or metallic compounds, making the use of such substances
29
30
31 1051 questionable. Thus, combining other solutions such as organic polymers and topography can be an
32
33
34
35 1052 efficient mode of action.
36
37
38

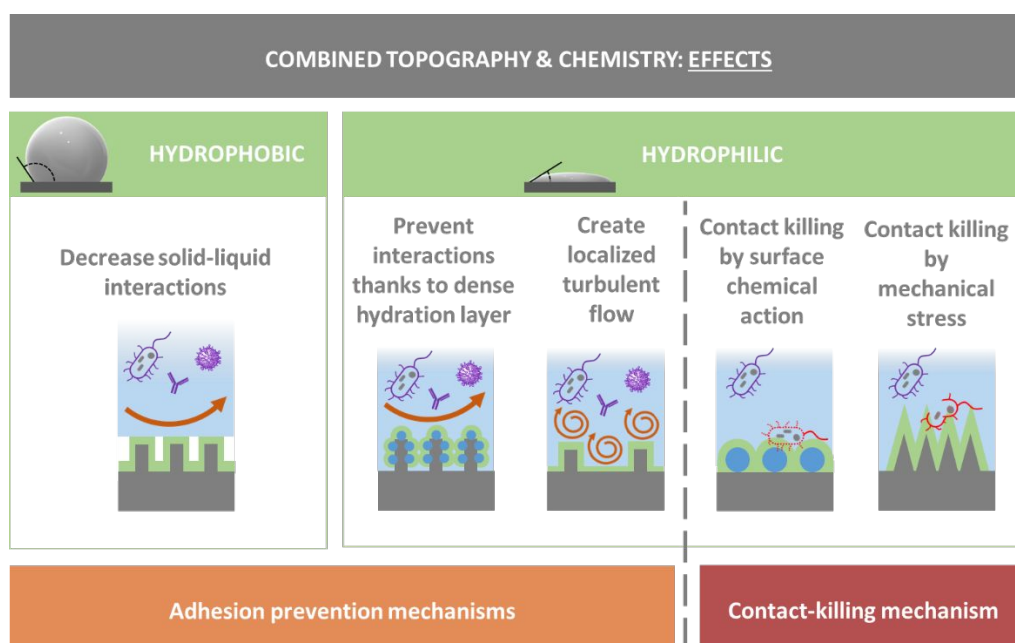
39 1053 More precisely, macromolecules with hydrophobic or hydrophilic properties show great interest
40
41
42 1054 for their ability to stop bacterial adhesion, and their activity can be enhanced by coating them on
43
44
45
46 1055 micro or nanostructured surfaces. In addition to increasing the wettability effect of certain
47
48
49 1056 substances, some structured surfaces can cause bacterial membranes to rupture through mechanical
50
51
52
53 1057 deformation. Others can lead to hydrodynamic fluxes which inhibit bacterial sedimentation and
54
55
56
57
58
59
60

1
2
3
4 1058 thus, biofouling. Precise control over the size and shape of the used structures could enable better
5
6
7 1059 understanding of their effect on bacterial adhesion and could also facilitate the adaptation of the
8
9
10 1060 surfaces to different strains of bacteria. Some structures could have opposite and non-desired
11
12
13 1061 effects and serve as bacterial traps. Concerning hydrophilic substances, depending on their nature,
14
15
16
17 1062 bactericidal properties can also be observed. All of these mechanisms are represented in Figure 15
18
19
20 1063 which highlights the diversity of action of hydrophilicity-based approaches in comparison to
21
22
23 1064 hydrophobic strategies based on the Cassie-Baxter regime.

24
25
26
27
28 1065 As emphasized by the organisation of this review, the initial material used for creating these
29
30
31 1066 antibiofouling surfaces with a combined approach can be metallic, glass or a variety of polymers.
32
33
34 1067 The adaptability to various substrates is interesting to address the wide range of applications where
35
36
37
38 1068 antibiofouling surfaces are needed.

39
40
41
42 1069 However, despite all the different solutions discovered while writing this review and summarized
43
44
45 1070 in Table S2 and S3, there seems to be a lack of statistical experiments. Indeed, here, independent
46
47
48
49 1071 experiments have been carried out with one combination of polymer and topography and one or
50
51
52 1072 two species of bacteria. This lack of systematic studies has been noticed by other teams and projects
53
54
55
56 1073 are arising. Indeed, Linklater *et al* have published in February 2022 a first statistical study of the
57
58
59

1
2
3
4 1074 effect of different nanopillar polymers on *P. aeruginosa* and *S. aureus*.⁹⁵ Furthermore, oppositely
5
6
7 1075 to *in vitro* experiments, in natural environments, one species of bacteria, or one marine species is
8
9
10 1076 rarely found alone, rather in a mixture with many other organisms. Only a few of the articles in this
11
12
13 1077 review have mentioned experiments carried out with natural samples. Therefore we can wonder
14
15
16
17 1078 whether transposing any of these modified surfaces to other applications would prove efficient or
18
19
20 1079 if the substrate would always have to be adapted to the field of interest and to the particular device.
21
22
23



1081 *Figure 15: Diverse effects of surface modification approaches for antibiofouling, and corresponding*
1082 *mechanisms*

1083 To verify the biocompatibility of these surfaces created with the prospect of replacing possible
1084 toxic solutions, cytotoxicity experiments need to be carried out in parallel. This aspect can be

1
2
3
4 1085 critical in some domains such as medical implants, where a risk of damaging human cells is
5
6
7 1086 unconceivable. It is also important in the marine industry to protect the natural fauna and flora. In
8
9
10 1087 this review, most of the publications using hydrophobicity to inhibit biofilm formation use fluorine-
11
12
13 1088 based chemicals. However, concern over the negative impacts of some fluorine-containing
14
15
16
17 1089 compounds could lead to an increase in fluorine-free surface development in the near future.
18
19
20
21 1090 Finally, the question of the robustness and durability of these surfaces should also be studied to
22
23
24 1091 verify their applicability *in vivo*. Indeed, biofilm is created rapidly but becomes stronger overtime.
25
26
27
28 1092 For a device left in a liquid medium over several months, it is very important that its efficiency
29
30
31 1093 does not degrade in that time. These durability assays should also be adapted depending on the
32
33
34 1094 application as the stress applied to a device could be very different.
35
36
37
38
39 1095 Overall, although complimentary research still needs to be carried out to respond to the yet
40
41
42 1096 unanswered questions, combining chemistry and topography seems to be a promising strategy to
43
44
45
46 1097 reach environmentally friendly, biocompatible and antibiofouling surfaces.
47
48
49

50 1098 SUPPORTING INFORMATION:
51
52
53
54
55
56
57
58
59
60

1
2
3 1099 Table S1 showing recent review articles on antibiofouling surfaces and overview tables (S2 & S3)

4
5
6
7 1100 summarizing the combined strategies described in this manuscript.

8
9
10 1101

11
12
13 1102 AUTHOR INFORMATION

14
15
16
17 1103 **Corresponding Author**

18
19
20
21 1104 Hippolyte Durand, hippolyte.durand@cea.fr

22
23
24
25 1105 **Present Addresses**

26
27
28
29 1106 CEA LETI Grenoble - DRT/DTBS, 17 avenue des martyrs, 38054, Grenoble cedex 9, France

30
31
32
33 1107 **Author Contributions**

34
35
36 1108 The manuscript was written through contributions of all authors. Miss Whiteley and Mr. Durand

37
38
39 1109 were in charge of the gathering and analysis of the relevant articles, and of the writing of the

40
41
42
43 1110 manuscript. Mr. Mailley participated in the reviewing process and brought insights for the

44
45
46 1111 manuscript structure, in addition to corrections. Mr. Nonglaton participated to the development of

47
48
49 1112 the manuscript structure and scope, in addition to corrections. All authors have given approval to

50
51
52
53 1113 the final version of the manuscript.

1
2
3
4 1114 ‡These authors contributed equally.
5
6
7

8 1115 **Funding Sources**
9

10
11
12 1116 **Notes**
13
14

15 1117 **ACKNOWLEDGMENT**
16
17

18 1118 The authors acknowledge the support of the Agence Nationale de la Recherche through the LabEx
19 1119 ARCANE program (ANR-11-LABX-0003-01) and the Graduate School on Chemistry, Biology
20 1120 and Health of Univ Grenoble Alpes CBH-EUR-GS (ANR-17-EURE-0003).
21
22
23

24 1121 **ABBREVIATIONS**
25
26
27

28 1122 *Abbreviations are all explained in the text*
29
30
31

32 1123 **REFERENCES**
33
34

- 35 1124 (1) Nunes, S. P. Can Fouling in Membranes Be Ever Defeated? *Current Opinion in Chemical*
36 1125 *Engineering* **2020**, *28*, 90–95. <https://doi.org/10.1016/j.coche.2020.03.006>.
37
38 1126 (2) Hopkins, G.; Davidson, I.; Georgiades, E.; Floerl, O.; Morrisey, D.; Cahill, P. Managing
39 1127 Biofouling on Submerged Static Artificial Structures in the Marine Environment –
40 1128 Assessment of Current and Emerging Approaches. *Frontiers in Marine Science* **2021**, *8*,
41 1129 1507. <https://doi.org/10.3389/fmars.2021.759194>.
42 1130 (3) Davidson, I.; Cahill, P.; Hinz, A.; Kluza, D.; Scianni, C.; Georgiades, E. A Review of
43 1131 Biofouling of Ships' Internal Seawater Systems. *Frontiers in Marine Science* **2021**, *8*, 1590.
44 1132 <https://doi.org/10.3389/fmars.2021.761531>.
45 1133 (4) Saget, M.; Almeida, C. F. de; Fierro, V.; Celzard, A.; Delaplace, G.; Thomy, V.; Coffinier,
46 1134 Y.; Jimenez, M. A Critical Review on Surface Modifications Mitigating Dairy Fouling.
47 1135 *Comprehensive Reviews in Food Science and Food Safety* **2021**, *n/a* (n/a).
48 1136 <https://doi.org/10.1111/1541-4337.12794>.
49
50
51
52
53
54
55
56
57
58
59
60

- 1
2
3
4 1137 (5) Wang, Y.; Wang, F.; Zhang, H.; Yu, B.; Cong, H.; Shen, Y. Antibacterial Material
5 1138 Surfaces/Interfaces for Biomedical Applications. *Applied Materials Today* **2021**, *25*,
6 1139 101192. <https://doi.org/10.1016/j.apmt.2021.101192>.
- 8 1140 (6) Zhou, L.; Wong, H. M.; Li, Q. L. Anti-Biofouling Coatings on the Tooth Surface and
9 1141 Hydroxyapatite. *Int. J. Nanomed.* **2020**, *15*, 8963–8982.
11 1142 <https://doi.org/10.2147/IJN.S281014>.
- 13 1143 (7) Balaure, P. C.; Grumezescu, A. M. Recent Advances in Surface Nanoengineering for
14 1144 Biofilm Prevention and Control. Part II: Active, Combined Active and Passive, and Smart
15 1145 Bacteria-Responsive Antibiofilm Nanocoatings. *Nanomaterials* **2020**, *10* (8), 1–53.
16 1146 <https://doi.org/10.3390/nano10081527>.
- 20 1147 (8) *New report calls for urgent action to avert antimicrobial resistance crisis.*
21 1148 [https://www.who.int/news/item/29-04-2019-new-report-calls-for-urgent-action-to-avert-](https://www.who.int/news/item/29-04-2019-new-report-calls-for-urgent-action-to-avert-antimicrobial-resistance-crisis)
22 1149 [antimicrobial-resistance-crisis](https://www.who.int/news/item/29-04-2019-new-report-calls-for-urgent-action-to-avert-antimicrobial-resistance-crisis) (accessed 2022-05-20).
- 25 1150 (9) *European Commission, Public Health, Antimicrobial Resistance, AMR: a major European*
26 1151 *and Global challenge.* European Commission 2017.
27 1152 [https://ec.europa.eu/health/document/download/87c8d30b-d23d-496f-b0c7-](https://ec.europa.eu/health/document/download/87c8d30b-d23d-496f-b0c7-a757102774b3_en)
28 1153 [a757102774b3_en](https://ec.europa.eu/health/document/download/87c8d30b-d23d-496f-b0c7-a757102774b3_en) (accessed 2022-06-23).
- 32 1154 (10) Gupta, P.; Bhatia, M.; Gupta, P.; Omar, B. J. Emerging Biocide Resistance among
33 1155 Multidrug-Resistant Bacteria: Myth or Reality? A Pilot Study. *J Pharm Bioallied Sci* **2018**,
34 1156 *10*(2), 96–101. https://doi.org/10.4103/JPBS.JPBS_24_18.
- 37 1157 (11) Sethi, S. K.; Manik, G. Recent Progress in Super Hydrophobic/Hydrophilic Self-Cleaning
38 1158 Surfaces for Various Industrial Applications: A Review. *Polymer-Plastics Technology and*
39 1159 *Engineering* **2018**, *57*(18), 1932–1952. <https://doi.org/10.1080/03602559.2018.1447128>.
- 42 1160 (12) Batista-Andrade, J. A.; Caldas, S. S.; Batista, R. M.; Castro, I. B.; Fillmann, G.; Primel, E.
43 1161 G. From TBT to Booster Biocides: Levels and Impacts of Antifouling along Coastal Areas
44 1162 of Panama. *Environmental Pollution* **2018**, *234*, 243–252.
45 1163 <https://doi.org/10.1016/j.envpol.2017.11.063>.
- 48 1164 (13) Adlhart, C.; Verran, J.; Azevedo, N. F.; Olmez, H.; Keinänen-Toivola, M. M.; Gouveia, I.;
49 1165 Melo, L. F.; Crijns, F. Surface Modifications for Antimicrobial Effects in the Healthcare
50 1166 Setting: A Critical Overview. *Journal of Hospital Infection* **2018**, *99* (3), 239–249.
51 1167 <https://doi.org/10.1016/j.jhin.2018.01.018>.

- 1
2
3
4 1168 (14) Ahmadabadi, H. Y.; Yu, K.; Kizhakkedathu, J. N. Surface Modification Approaches for
5 1169 Prevention of Implant Associated Infections. *Colloids and Surfaces B: Biointerfaces* **2020**,
6 1170 *193*, 111116. <https://doi.org/10.1016/j.colsurfb.2020.111116>.
- 7
8 1171 (15) Modaresifar, K.; Azizian, S.; Ganjian, M.; Fratila-Apachitei, L. E.; Zadpoor, A. A.
9 1172 Bactericidal Effects of Nanopatterns: A Systematic Review. *Acta Biomaterialia* **2019**, *83*,
10 1173 29–36. <https://doi.org/10.1016/j.actbio.2018.09.059>.
- 11
12 1174 (16) Echeverria, C.; Torres, M. D. T.; Fernández-García, M.; de la Fuente-Nunez, C.; Muñoz-
13 1175 Bonilla, A. Physical Methods for Controlling Bacterial Colonization on Polymer Surfaces.
14 1176 *Biotechnology Advances* **2020**, *43*, 107586.
15 1177 <https://doi.org/10.1016/j.biotechadv.2020.107586>.
- 16
17 1178 (17) Halder, P.; Hossain, N.; Pramanik, B. K.; Bhuiyan, M. A. Engineered Topographies and
18 1179 Hydrodynamics in Relation to Biofouling Control—a Review. *Environ Sci Pollut Res* **2020**,
19 1180 *28*, 40678–40692. <https://doi.org/10.1007/s11356-020-10864-3>.
- 20
21 1181 (18) He, M.; Gao, K.; Zhou, L.; Jiao, Z.; Wu, M.; Cao, J.; You, X.; Cai, Z.; Su, Y.; Jiang, Z.
22 1182 Zwitterionic Materials for Antifouling Membrane Surface Construction. *Acta Biomaterialia*
23 1183 **2016**, *40*, 142–152. <https://doi.org/10.1016/j.actbio.2016.03.038>.
- 24
25 1184 (19) Lim, C.-M.; Li, M.-X.; Joung, Y. K. Surface-Modifying Polymers for Blood-Contacting
26 1185 Polymeric Biomaterials. In *Biomimicked Biomaterials: Advances in Tissue Engineering and*
27 1186 *Regenerative Medicine*; Chun, H. J., Reis, R. L., Motta, A., Khang, G., Eds.; Advances in
28 1187 Experimental Medicine and Biology; Springer: Singapore, 2020; pp 189–198.
29 1188 https://doi.org/10.1007/978-981-15-3262-7_13.
- 30
31 1189 (20) Shahsavan, H.; Arunbabu, D.; Zhao, B. Biomimetic Modification of Polymeric Surfaces: A
32 1190 Promising Pathway for Tuning of Wetting and Adhesion. *Macromolecular Materials and*
33 1191 *Engineering* **2012**, *297*(8), 743–760. <https://doi.org/10.1002/mame.201200016>.
- 34
35 1192 (21) Sullivan, T.; O’Callaghan, I. Recent Developments in Biomimetic Antifouling Materials: A
36 1193 Review. *Biomimetics* **2020**, *5*(4), 58. <https://doi.org/10.3390/biomimetics5040058>.
- 37
38 1194 (22) Mas-Moruno, C.; Su, B.; Dalby, M. J. Multifunctional Coatings and Nanotopographies:
39 1195 Toward Cell Instructive and Antibacterial Implants. *Advanced Healthcare Materials* **2019**,
40 1196 *8*(1), 1801103. <https://doi.org/10.1002/adhm.201801103>.
- 41
42 1197 (23) Shi, Y.; Liu, K.; Zhang, Z.; Tao, X.; Chen, H.-Y.; Kingshott, P.; Wang, P.-Y. Decoration of
43 1198 Material Surfaces with Complex Physicochemical Signals for Biointerface Applications.

- 1
2
3
4 1199 *ACS Biomater. Sci. Eng.* **2020**, *6* (4), 1836–1851.
5 1200 <https://doi.org/10.1021/acsbiomaterials.9b01806>.
6
7 1201 (24) Chen, L.; Duan, Y.; Cui, M.; Huang, R.; Su, R.; Qi, W.; He, Z. Biomimetic Surface Coatings
8 1202 for Marine Antifouling: Natural Antifoulants, Synthetic Polymers and Surface
9 1203 Microtopography. *Science of The Total Environment* **2021**, *766*, 144469.
10 1204 <https://doi.org/10.1016/j.scitotenv.2020.144469>.
11
12 1205 (25) Védie, E.; Brisset, H.; Briand, J.-F.; Bressy, C. Bioinspiration and Microtopography As
13 1206 Nontoxic Strategies for Marine Bioadhesion Control. *Advanced Materials Interfaces* **2021**,
14 1207 *n/a* (n/a), 2100994. <https://doi.org/10.1002/admi.202100994>.
15
16 1208 (26) Kumar, A.; AL-Jumaili, A.; Bazaka, O.; Ivanova, E. P.; Levchenko, I.; Bazaka, K.; Jacob,
17 1209 M. V. Functional Nanomaterials, Synergisms, and Biomimicry for Environmentally Benign
18 1210 Marine Antifouling Technology. *Mater. Horiz.* **2021**, *8*, 3201–3238.
19 1211 <https://doi.org/10.1039/D1MH01103K>.
20
21 1212 (27) Larrañaga-Altuna, M.; Zabala, A.; Llavori, I.; Pearce, O.; Nguyen, D. T.; Caro, J.;
22 1213 Mescheder, H.; Endrino, J. L.; Goel, G.; Ayre, W. N.; Seenivasagam, R. K.; Tripathy, D. K.;
23 1214 Armstrong, J.; Goel, S. Bactericidal Surfaces: An Emerging 21st-Century Ultra-Precision
24 1215 Manufacturing and Materials Puzzle. *Applied Physics Reviews* **2021**, *8* (2), 021303.
25 1216 <https://doi.org/10.1063/5.0028844>.
26
27 1217 (28) Kung, C. H.; Sow, P. K.; Zahiri, B.; Mérida, W. Assessment and Interpretation of Surface
28 1218 Wettability Based on Sessile Droplet Contact Angle Measurement: Challenges and
29 1219 Opportunities. *Advanced Materials Interfaces* **2019**, *6* (18), 1900839.
30 1220 <https://doi.org/10.1002/admi.201900839>.
31
32 1221 (29) Tran, P. A.; Webster, T. J. Understanding the Wetting Properties of Nanostructured
33 1222 Selenium Coatings: The Role of Nanostructured Surface Roughness and Air-Pocket
34 1223 Formation. *International Journal of Nanomedicine* **2013**, 2001–2009.
35
36 1224 (30) Moazzam, P.; Razmjou, A.; Golabi, M.; Shokri, D.; Landarani-Isfahani, A. Investigating the
37 1225 BSA Protein Adsorption and Bacterial Adhesion of Al-Alloy Surfaces after Creating a
38 1226 Hierarchical (Micro/Nano) Superhydrophobic Structure. *Journal of Biomedical Materials*
39 1227 *Research Part A* **2016**, *104* (9), 2220–2233. <https://doi.org/10.1002/jbm.a.35751>.
40
41 1228 (31) Mandal, P.; Shishodia, A.; Ali, N.; Ghosh, S.; Arora, H. S.; Grewal, H. S.; Ghosh, S. K.
42 1229 Effect of Topography and Chemical Treatment on the Hydrophobicity and Antibacterial
43
44
45
46
47
48
49
50
51
52
53
54
55
56
57
58
59
60

- 1
2
3
4 1230 Activities of Micropatterned Aluminium Surfaces. *Surf. Topogr.: Metrol. Prop.* **2020**, *8* (2),
5 1231 025017. <https://doi.org/10.1088/2051-672X/ab8d86>.
6
7 1232 (32) Mandal, P.; Ivvala, J.; Arora, H. S.; Ghosh, S. K.; Grewal, H. S. Bioinspired Micro/Nano
8 1233 Structured Aluminum with Multifaceted Applications. *Colloids and Surfaces B:*
9 1234 *Biointerfaces* **2022**, *211*, 112311. <https://doi.org/10.1016/j.colsurfb.2021.112311>.
10 1235 (33) Wang, M.; Zi, Y.; Zhu, J.; Huang, W.; Zhang, Z.; Zhang, H. Construction of Super-
11 1236 Hydrophobic PDMS@MOF@Cu Mesh for Reduced Drag, Anti-Fouling and Self-Cleaning
12 1237 towards Marine Vehicle Applications. *Chemical Engineering Journal* **2021**, *417*, 129265.
13 1238 <https://doi.org/10.1016/j.cej.2021.129265>.
14 1239 (34) Chen, F.; Zhang, D.; Yang, Q.; Yong, J.; Du, G.; Si, J.; Yun, F.; Hou, X. Bioinspired Wetting
15 1240 Surface via Laser Microfabrication. *ACS Appl. Mater. Interfaces* **2013**, *5* (15), 6777–6792.
16 1241 <https://doi.org/10.1021/am401677z>.
17 1242 (35) Vorobyev, A. Y.; Guo, C. Direct Femtosecond Laser Surface Nano/Microstructuring and Its
18 1243 Applications. *Laser & Photonics Reviews* **2013**, *7* (3), 385–407.
19 1244 <https://doi.org/10.1002/lpor.201200017>.
20 1245 (36) Li, S.; Liu, Y.; Zheng, Z.; Liu, X.; Huang, H.; Han, Z.; Ren, L. Biomimetic Robust
21 1246 Superhydrophobic Stainless-Steel Surfaces with Antimicrobial Activity and Molecular
22 1247 Dynamics Simulation. *Chemical Engineering Journal* **2019**, *372*, 852–861.
23 1248 <https://doi.org/10.1016/j.cej.2019.04.200>.
24 1249 (37) Zouaghi, S.; Six, T.; Bellayer, S.; Coffinier, Y.; Abdallah, M.; Chihib, N.-E.; André, C.;
25 1250 Delaplace, G.; Jimenez, M. Atmospheric Pressure Plasma Spraying of Silane-Based
26 1251 Coatings Targeting Whey Protein Fouling and Bacterial Adhesion Management. *Applied*
27 1252 *Surface Science* **2018**, *455*, 392–402. <https://doi.org/10.1016/j.apsusc.2018.06.006>.
28 1253 (38) Zouaghi, S.; Bellayer, S.; Thomy, V.; Dargent, T.; Coffinier, Y.; Andre, C.; Delaplace, G.;
29 1254 Jimenez, M. Biomimetic Surface Modifications of Stainless Steel Targeting Dairy Fouling
30 1255 Mitigation and Bacterial Adhesion. *Food and Bioproducts Processing* **2019**, *113*, 32–38.
31 1256 <https://doi.org/10.1016/j.fbp.2018.10.012>.
32 1257 (39) Tuo, Y.; Zhang, H.; Chen, L.; Chen, W.; Liu, X.; Song, K. Fabrication of Superamphiphobic
33 1258 Surface with Hierarchical Structures on Metal Substrate. *Colloids and Surfaces A:*
34 1259 *Physicochemical and Engineering Aspects* **2021**, *612*, 125983.
35 1260 <https://doi.org/10.1016/j.colsurfa.2020.125983>.
36
37
38
39
40
41
42
43
44
45
46
47
48
49
50
51
52
53
54
55
56
57
58
59
60

- 1
2
3
4 1261 (40) Cao, P.; Du, C.; He, X.; Zhang, C.; Yuan, C. Modification of a Derived Antimicrobial
5 1262 Peptide on Steel Surface for Marine Bacterial Resistance. *Applied Surface Science* **2020**,
6 1263 *510*, 145512. <https://doi.org/10.1016/j.apsusc.2020.145512>.
- 8 1264 (41) Gu, T.; Meesrisom, A.; Luo, Y.; Dinh, Q. N.; Lin, S.; Yang, M.; Sharma, A.; Tang, R.;
9 1265 Zhang, J.; Jia, Z.; Millner, P. D.; Pearlstein, A. J.; Zhang, B. *Listeria Monocytogenes* Biofilm
10 1266 Formation as Affected by Stainless Steel Surface Topography and Coating Composition.
11 1267 *Food Control* **2021**, *130*, 108275. <https://doi.org/10.1016/j.foodcont.2021.108275>.
- 15 1268 (42) Bao, Y.; Fu, W.; Xu, H.; Chen, Y.; Zhang, H.; Chen, S. Bioinspired Self-Cleaning Surface
16 1269 with Microflower-like Structures Constructed by Electrochemically Corrosion Mediated
17 1270 Self-Assembly. *CrystEngComm* **2021**, *24*, 1085–1093.
18 1271 <https://doi.org/10.1039/D1CE01267C>.
- 22 1272 (43) Lee, J.; Jiang, Y.; Hizal, F.; Ban, G.-H.; Jun, S.; Choi, C.-H. Durable Omniphobicity of Oil-
23 1273 Impregnated Anodic Aluminum Oxide Nanostructured Surfaces. *Journal of Colloid and*
24 1274 *Interface Science* **2019**, *553*, 734–745. <https://doi.org/10.1016/j.jcis.2019.06.068>.
- 27 1275 (44) Lee, J.; Wooh, S.; Choi, C.-H. Fluorocarbon Lubricant Impregnated Nanoporous Oxide for
28 1276 Omnicorrosion-Resistant Stainless Steel. *Journal of Colloid and Interface Science* **2020**,
29 1277 *558*, 301–309. <https://doi.org/10.1016/j.jcis.2019.09.117>.
- 32 1278 (45) Hizal, F.; Rungraeng, N.; Lee, J.; Jun, S.; Busscher, H. J.; van der Mei, H. C.; Choi, C.-H.
33 1279 Nanoengineered Superhydrophobic Surfaces of Aluminum with Extremely Low Bacterial
34 1280 Adhesivity. *ACS Appl. Mater. Interfaces* **2017**, *9* (13), 12118–12129.
35 1281 <https://doi.org/10.1021/acsami.7b01322>.
- 38 1282 (46) Chang, X.; Li, M.; Tang, S.; Shi, L.; Chen, X.; Niu, S.; Zhu, X.; Wang, D.; Sun, S.
39 1283 Superhydrophobic Micro-Nano Structured PTFE/WO₃ Coating on Low-Temperature Steel
40 1284 with Outstanding Anti-Pollution, Anti-Icing, and Anti-Fouling Performance. *Surface and*
41 1285 *Coatings Technology* **2022**, *434*, 128214. <https://doi.org/10.1016/j.surfcoat.2022.128214>.
- 45 1286 (47) Ouyang, Y.; Zhao, J.; Qiu, R.; Hu, S.; Chen, M.; Wang, P. Liquid-Infused Superhydrophobic
46 1287 Dendritic Silver Matrix: A Bio-Inspired Strategy to Prohibit Biofouling on Titanium.
47 1288 *Surface and Coatings Technology* **2019**, *367*, 148–155.
48 1289 <https://doi.org/10.1016/j.surfcoat.2019.03.067>.
- 52 1290 (48) Bruzard, J.; Tarrade, J.; Celia, E.; Darmanin, T.; Taffin de Givenchy, E.; Guittard, F.; Herry,
53 1291 J.-M.; Guilbaud, M.; Bellon-Fontaine, M.-N. The Design of Superhydrophobic Stainless
54 1292 Steel Surfaces by Controlling Nanostructures: A Key Parameter to Reduce the Implantation

- 1
2
3
4 1293 of Pathogenic Bacteria. *Materials Science and Engineering: C* **2017**, *73*, 40–47.
5 1294 <https://doi.org/10.1016/j.msec.2016.11.115>.
6
7 1295 (49) Li, J.; Yuan, T.; Zhou, C.; Chen, B.; Shuai, Y.; Wu, D.; Chen, D.; Luo, X.; Cheng, Y. F.;
8 1296 Liu, Y. Facile Li-Al Layered Double Hydroxide Films on Al Alloy for Enhanced
9 1297 Hydrophobicity, Anti-Biofouling and Anti-Corrosion Performance. *Journal of Materials*
10 1298 *Science & Technology* **2021**, *79*, 230–242. <https://doi.org/10.1016/j.jmst.2020.10.072>.
11
12 1299 (50) Selim, M. S.; El-Safty, S. A.; Fatthallah, N. A.; Shenashen, M. A. Silicone/Graphene Oxide
13 1300 Sheet-Alumina Nanorod Ternary Composite for Superhydrophobic Antifouling Coating.
14 1301 *Progress in Organic Coatings* **2018**, *121*, 160–172.
15 1302 <https://doi.org/10.1016/j.porgcoat.2018.04.021>.
16
17 1303 (51) Selim, M. S.; Yang, H.; Wang, F. Q.; Fatthallah, N. A.; Huang, Y.; Kuga, S. Silicone/ZnO
18 1304 Nanorod Composite Coating as a Marine Antifouling Surface. *Applied Surface Science*
19 1305 **2019**, *466*, 40–50. <https://doi.org/10.1016/j.apsusc.2018.10.004>.
20
21 1306 (52) Lee, Y.; Chung, Y.-W.; Park, J.; Park, K.; Seo, Y.; Hong, S.-N.; Lee, S. H.; Jeon, H.; Seo,
22 1307 J. Lubricant-Infused Directly Engraved Nano-Microstructures for Mechanically Durable
23 1308 Endoscope Lens with Anti-Biofouling and Anti-Fogging Properties. *Scientific Reports*
24 1309 **2020**, *10*(1), 17454. <https://doi.org/10.1038/s41598-020-74517-8>.
25
26 1310 (53) Jiang, R.; Hao, L.; Song, L.; Tian, L.; Fan, Y.; Zhao, J.; Liu, C.; Ming, W.; Ren, L. Lotus-
27 1311 Leaf-Inspired Hierarchical Structured Surface with Non-Fouling and Mechanical
28 1312 Bactericidal Performances. *Chemical Engineering Journal* **2020**, *398*, 125609.
29 1313 <https://doi.org/10.1016/j.cej.2020.125609>.
30
31 1314 (54) Crick, C. R.; Ismail, S.; Pratten, J.; Parkin, I. P. An Investigation into Bacterial Attachment
32 1315 to an Elastomeric Superhydrophobic Surface Prepared via Aerosol Assisted Deposition.
33 1316 *Thin Solid Films* **2011**, *519*(11), 3722–3727. <https://doi.org/10.1016/j.tsf.2011.01.282>.
34
35 1317 (55) Privett, B.; J, Y.; Sa, H.; J, L.; J, H.; Jh, S.; Mh, S. Antibacterial Fluorinated Silica Colloid
36 1318 Superhydrophobic Surfaces. *Langmuir* **2011**, *27* (15), 9597–9601.
37 1319 <https://doi.org/10.1021/la201801e>.
38
39 1320 (56) Marguier, A.; Poulin, N.; Soraru, C.; Vonna, L.; Hajjar-Garreau, S.; Kunemann, P.; Airoudj,
40 1321 A.; Mertz, G.; Bardon, J.; Delmée, M.; Roucoules, V.; Ruch, D.; Ploux, L. Bacterial
41 1322 Colonization of Low-Wettable Surfaces Is Driven by Culture Conditions and Topography.
42 1323 *Advanced Materials Interfaces* **2020**, *n/a* (n/a), 2000179.
43 1324 <https://doi.org/10.1002/admi.202000179>.
44
45
46
47
48
49
50
51
52
53
54
55
56
57
58
59
60

- 1
2
3
4 1325 (57) Ware, C. S.; Smith-Palmer, T.; Peppou-Chapman, S.; Scarratt, L. R. J.; Humphries, E. M.;
5 1326 Balzer, D.; Neto, C. Marine Antifouling Behavior of Lubricant-Infused Nanowrinkled
6 1327 Polymeric Surfaces. *ACS Appl. Mater. Interfaces* **2018**, *10* (4), 4173–4182.
7 1328 <https://doi.org/10.1021/acsami.7b14736>.
- 8
9
10 1329 (58) Dolid, A.; Gomes, L. C.; Mergulhão, F. J.; Reches, M. Combining Chemistry and
11 1330 Topography to Fight Biofilm Formation: Fabrication of Micropatterned Surfaces with a
12 1331 Peptide-Based Coating. *Colloids and Surfaces B: Biointerfaces* **2020**, *196*, 111365.
13 1332 <https://doi.org/10.1016/j.colsurfb.2020.111365>.
- 14
15 1333 (59) Wu, Q.; Liu, D.; Chen, W.; Chen, H.; Yang, C.; Li, X.; Yang, C.; Lin, H.; Chen, S.; Hu, N.;
16 1334 Chen, W.; Xie, X. Liquid-like Layer Coated Intraocular Lens for Posterior Capsular
17 1335 Opacification Prevention. *Applied Materials Today* **2021**, *23*, 100981.
18 1336 <https://doi.org/10.1016/j.apmt.2021.100981>.
- 19
20 1337 (60) Kefallinou, D.; Ellinas, K.; Speliotis, T.; Stamatakis, K.; Gogolides, E.; Tserepi, A.
21 1338 Optimization of Antibacterial Properties of “Hybrid” Metal-Sputtered Superhydrophobic
22 1339 Surfaces. *Coatings* **2020**, *10*(1), 25. <https://doi.org/10.3390/coatings10010025>.
- 23
24 1340 (61) Fay, F.; Poncin-Epaillard, F.; Le Norcy, T.; Linossier, I.; Réhel, K. Surface Plasma
25 1341 Treatment (Ar/CF₄) Decreases Biofouling on Polycarbonate Surfaces. *Surface Innovations*
26 1342 **2020**, *9*(1), 65–76. <https://doi.org/10.1680/jsuin.20.00026>.
- 27
28 1343 (62) Chen, T.-L.; Lin, Y.-P.; Chien, C.-H.; Chen, Y.-C.; Yang, Y.-J.; Wang, W.-L.; Chien, L.-F.;
29 1344 Hsueh, H.-Y. Fabrication of Frog-Skin-Inspired Slippery Antibiofouling Coatings Through
30 1345 Degradable Block Copolymer Wrinkling. *Advanced Functional Materials* **2021**, *n/a* (n/a),
31 1346 2104173. <https://doi.org/10.1002/adfm.202104173>.
- 32
33 1347 (63) Seth, M.; Jana, S. Fabrication and Multifunctional Properties of Fluorine-Free Durable
34 1348 Nickel Stearate Based Superhydrophobic Cotton Fabric. *J Coat Technol Res* **2022**, *19*, 813–
35 1349 827. <https://doi.org/10.1007/s11998-021-00559-w>.
- 36
37 1350 (64) Song, L.; Sun, L.; Zhao, J.; Wang, X.; Yin, J.; Luan, S.; Ming, W. Synergistic
38 1351 Superhydrophobic and Photodynamic Cotton Textiles with Remarkable Antibacterial
39 1352 Activities. *ACS Appl. Bio Mater.* **2019**, *2* (7), 2756–2765.
40 1353 <https://doi.org/10.1021/acsabm.9b00149>.
- 41
42 1354 (65) Li, B.; Yun, Y.; Wang, M.; Li, C.; Yang, W.; Li, J.; Liu, G. Superhydrophobic Polymer
43 1355 Membrane Coated by Mineralized β -FeOOH Nanorods for Direct Contact Membrane
44 1356 Distillation. *Desalination* **2021**, *500*, 114889. <https://doi.org/10.1016/j.desal.2020.114889>.

- 1
2
3
4 1357 (66) Anjum, A. S.; Sun, K. C.; Ali, M.; Riaz, R.; Jeong, S. H. Fabrication of Coral-Reef
5 1358 Structured Nano Silica for Self-Cleaning and Super-Hydrophobic Textile Applications.
6
7 1359 *Chemical Engineering Journal* **2020**, *401*, 125859.
8
9 1360 <https://doi.org/10.1016/j.cej.2020.125859>.
- 10 1361 (67) Wang, T.; Huang, L.; Liu, Y.; Li, X.; Liu, C.; Handschuh-Wang, S.; Xu, Y.; Zhao, Y.; Tang,
11 1362 Y. Robust Biomimetic Hierarchical Diamond Architecture with a Self-Cleaning,
12 1363 Antibacterial, and Antibiofouling Surface. *ACS Appl. Mater. Interfaces* **2020**, *12* (21),
13 1364 24432–24441. <https://doi.org/10.1021/acsami.0c02460>.
- 14 1365 (68) Fang, Y.; Yong, J.; Cheng, Y.; Yang, Q.; Hou, X.; Chen, F. Liquid-Infused Slippery
15 1366 Stainless Steel Surface Prepared by Alcohol-Assisted Femtosecond Laser Ablation.
16 1367 *Advanced Materials Interfaces* **2021**, *8* (5), 2001334.
17 1368 <https://doi.org/10.1002/admi.202001334>.
- 18 1369 (69) An, R.; Dong, Y.; Zhu, J.; Rao, C. Adhesion and Friction Forces in Biofouling Attachments
19 1370 to Nanotube- and PEG- Patterned TiO₂ Surfaces. *Colloids and Surfaces B: Biointerfaces*
20 1371 **2017**, *159*, 108–117. <https://doi.org/10.1016/j.colsurfb.2017.07.067>.
- 21 1372 (70) Chen, X.; He, X.; Suo, X.; Huang, J.; Gong, Y.; Liu, Y.; Li, H. Effect of Surface Topological
22 1373 Structure and Chemical Modification of Flame Sprayed Aluminum Coatings on the
23 1374 Colonization of *Cylindrotheca Closterium* on Their Surfaces | Elsevier Enhanced Reader.
24 1375 *Applied Surface Science* **2016**, *388*, 385–391. <https://doi.org/10.1016/j.apsusc.2015.12.141>.
- 25 1376 (71) Ren, X.; Guo, M.; Xue, L.; Zeng, Q.; Gao, X.; Xin, Y.; Xu, L.; Li, L. A Self-Cleaning
26 1377 Mucus-like and Hierarchical Ciliary Bionic Surface for Marine Antifouling. *Advanced*
27 1378 *Engineering Materials* **2020**, *22* (5), 1901198. <https://doi.org/10.1002/adem.201901198>.
- 28 1379 (72) Lou, T.; Bai, X.; He, X.; Yuan, C. Antifouling Performance Analysis of Peptide-Modified
29 1380 Glass Microstructural Surfaces. *Applied Surface Science* **2020**, 148384.
30 1381 <https://doi.org/10.1016/j.apsusc.2020.148384>.
- 31 1382 (73) Chen, C.; Enrico, A.; Pettersson, T.; Ek, M.; Herland, A.; Niklaus, F.; Stemme, G.; Wagberg,
32 1383 L. Bactericidal Surfaces Prepared by Femtosecond Laser Patterning and Layer-by-Layer
33 1384 Polyelectrolyte Coating | Elsevier Enhanced Reader. *Journal of Colloid and Interface*
34 1385 *Science* **2020**, *575*, 286–297. <https://doi.org/10.1016/j.jcis.2020.04.107>.
- 35 1386 (74) González-Henríquez, C. M.; Rodríguez-Umanzor, F. E.; Alegría-Gómez, M. N.; Terraza-
36 1387 Inostroza, C. A.; Martínez-Campos, E.; Cue-López, R.; Sarabia-Vallejos, M. A.; García-
37 1388 Herrera, C.; Rodríguez-Hernández, J. Wrinkling on Stimuli-Responsive Functional Polymer

- 1
2
3
4 1389 Surfaces as a Promising Strategy for the Preparation of Effective
5 1390 Antibacterial/Antibiofouling Surfaces. *Polymers* **2021**, *13* (23), 4262.
6
7 1391 <https://doi.org/10.3390/polym13234262>.
- 8
9 1392 (75) Liu, H.; Ma, Z.; Yang, W.; Pei, X.; Zhou, F. Facile Preparation of Structured Zwitterionic
10 1393 Polymer Substrate via Sub-Surface Initiated Atom Transfer Radical Polymerization and Its
11 1394 Synergistic Marine Antifouling Investigation. *European Polymer Journal* **2019**, *112*, 146–
12 1395 152. <https://doi.org/10.1016/j.eurpolymj.2018.07.025>.
- 13
14 1396 (76) Yu, X.; Yang, W.; Yang, Y.; Wang, X.; Liu, X.; Zhou, F.; Zhao, Y. Subsurface-Initiated
15 1397 Atom Transfer Radical Polymerization: Effect of Graft Layer Thickness and Surface
16 1398 Morphology on Antibiofouling Properties against Different Foulants. *J Mater Sci* **2020**, *55*
17 1399 (29), 14544–14557. <https://doi.org/10.1007/s10853-020-05055-x>.
- 18
19 1400 (77) Xu, X.; Wang, K.; Guo, H.; Sun, G.; Chen, R.; Yu, J.; Liu, J.; Lin, C.; Wang, J. Zwitterionic
20 1401 Modified Electrostatic Flocking Surfaces for Diatoms and Mussels Resistance. *Journal of*
21 1402 *Colloid and Interface Science* **2021**, *588*, 9–18. <https://doi.org/10.1016/j.jcis.2020.12.036>.
- 22 1403 (78) Zhang, Y.; Hu, H.; Pei, X.; Liu, Y.; Ye, Q.; Zhou, F. Polymer Brushes on Structural Surfaces:
23 1404 A Novel Synergistic Strategy for Perfectly Resisting Algae Settlement. *Biomater. Sci.* **2017**,
24 1405 *5*(12), 2493–2500. <https://doi.org/10.1039/C7BM00842B>.
- 25
26 1406 (79) Brzozowska, A. M.; Parra-Velandia, F. J.; Quintana, R.; Xiaoying, Z.; Lee, S. S. C.; Chin-
27 1407 Sing, L.; Jańczewski, D.; Teo, S. L.-M.; Vancso, J. G. Biomimicking Micropatterned
28 1408 Surfaces and Their Effect on Marine Biofouling. *Langmuir* **2014**, *30* (30), 9165–9175.
29 1409 <https://doi.org/10.1021/la502006s>.
- 30
31 1410 (80) Zhao, L.; Chen, R.; Lou, L.; Jing, X.; Liu, Q.; Liu, J.; Yu, J.; Liu, P.; Wang, J. Layer-by-
32 1411 Layer-Assembled Antifouling Films with Surface Microtopography Inspired by *Laminaria*
33 1412 *Japonica*. *Applied Surface Science* **2020**, *511*, 145564.
34 1413 <https://doi.org/10.1016/j.apsusc.2020.145564>.
- 35
36 1414 (81) Weinman, S. T.; Husson, S. M. Influence of Chemical Coating Combined with
37 1415 Nanopatterning on Alginate Fouling during Nanofiltration. *Journal of Membrane Science*
38 1416 **2016**, *513*, 146–154. <https://doi.org/10.1016/j.memsci.2016.04.025>.
- 39
40 1417 (82) Choi, W.; Chan, E. P.; Park, J.-H.; Ahn, W.-G.; Jung, H. W.; Hong, S.; Lee, J. S.; Han, J.-
41 1418 Y.; Park, S.; Ko, D.-H.; Lee, J.-H. Nanoscale Pillar-Enhanced Tribological Surfaces as
42 1419 Antifouling Membranes. *ACS Appl. Mater. Interfaces* **2016**, *8* (45), 31433–31441.
43 1420 <https://doi.org/10.1021/acsami.6b10875>.
- 44
45
46
47
48
49
50
51
52
53
54
55
56
57
58
59
60

- 1
2
3
4 1421 (83) Choi, W.; Lee, C.; Lee, D.; Won, Y. J.; Lee, G. W.; Shin, M. G.; Chun, B.; Kim, T.-S.; Park,
5 1422 H.-D.; Jung, H. W.; Lee, J. S.; Lee, J.-H. Sharkskin-Mimetic Desalination Membranes with
6 1423 Ultralow Biofouling. *J. Mater. Chem. A* **2018**, *6* (45), 23034–23045.
7 1424 <https://doi.org/10.1039/C8TA06125D>.
- 8
9
10 1425 (84) Choi, W.; Lee, C.; Yoo, C. H.; Shin, M. G.; Lee, G. W.; Kim, T.-S.; Jung, H. W.; Lee, J. S.;
11 1426 Lee, J.-H. Structural Tailoring of Sharkskin-Mimetic Patterned Reverse Osmosis
12 1427 Membranes for Optimizing Biofouling Resistance. *Journal of Membrane Science* **2020**, *595*,
13 1428 117602. <https://doi.org/10.1016/j.memsci.2019.117602>.
- 14
15
16
17 1429 (85) Choi, W.; Shin, M. G.; Yoo, C. H.; Park, H.; Park, Y.-I.; Lee, J. S.; Lee, J.-H. Desalination
18 1430 Membranes with Ultralow Biofouling via Synergistic Chemical and Topological Strategies.
19 1431 *Journal of Membrane Science* **2021**, *626*, 119212.
20 1432 <https://doi.org/10.1016/j.memsci.2021.119212>.
- 21
22
23
24 1433 (86) Zhao, L.; Zhang, M.; Liu, G.; Zhao, A.; Gong, X.; Shi, S.; Zheng, X.; Gao, J.; Jiang, Y.
25 1434 Tuning the Microstructure of a Zwitterion-Functionalized Polyethylenimine Loose NF
26 1435 Membrane for Dye Desalination. *Ind. Eng. Chem. Res.* **2022**, *61* (5), 2245–2256.
27 1436 <https://doi.org/10.1021/acs.iecr.1c04521>.
- 28
29
30
31 1437 (87) Aguilar-Sanchez, A.; Jalvo, B.; Mautner, A.; Rissanen, V.; Kontturi, K. S.; Abdelhamid, H.
32 1438 N.; Tammel, T.; Mathew, A. P. Charged Ultrafiltration Membranes Based on TEMPO-
33 1439 Oxidized Cellulose Nanofibrils/Poly(Vinyl Alcohol) Antifouling Coating. *RSC Adv.* **2021**,
34 1440 *11* (12), 6859–6868. <https://doi.org/10.1039/D0RA10220B>.
- 35
36
37 1441 (88) Lin, B.; Tan, H.; Liu, W.; Gao, C.; Pan, Q. Preparation of a Novel Zwitterionic Striped
38 1442 Surface Thin-Film Composite Nanofiltration Membrane with Excellent Salt Separation
39 1443 Performance and Antifouling Property. *RSC Advances* **2020**, *10* (27), 16168–16178.
40 1444 <https://doi.org/10.1039/D0RA00480D>.
- 41
42
43
44 1445 (89) Liu, Y.; Gao, J.; Ge, Y.; Yu, S.; Liu, M.; Gao, C. A Combined Interfacial Polymerization
45 1446 and In-Situ Sol-Gel Strategy to Construct Composite Nanofiltration Membrane with
46 1447 Improved Pore Size Distribution and Anti-Protein-Fouling Property. *Journal of Membrane*
47 1448 *Science* **2021**, *623*, 119097. <https://doi.org/10.1016/j.memsci.2021.119097>.
- 48
49
50
51 1449 (90) Ma, Z.; Liang, S.; Xiao, K.; Wang, X.; Li, M.; Huang, X. Superhydrophilic Polyvinylidene
52 1450 Fluoride Membrane with Hierarchical Surface Structures Fabricated via Nanoimprint and
53 1451 Nanoparticle Grafting. *Journal of Membrane Science* **2020**, *612*, 118332.
54 1452 <https://doi.org/10.1016/j.memsci.2020.118332>.
- 55
56
57
58
59
60

- 1
2
3
4 1453 (91) Sun, M.; Wu, Q.; Xu, J.; He, F.; Brown, A. P.; Ye, Y. Vapor-Based Grafting of Crosslinked
5 1454 Poly(N-Vinyl Pyrrolidone) Coatings with Tuned Hydrophilicity and Anti-Biofouling
6 1455 Properties†. *Journal of Materials Chemistry B* **2016**, No. 4, 2669.
7 1456 <https://doi.org/10.1039/c6tb00076b>.
- 8
9
10 1457 (92) Park, H.-H.; Sun, K.; Lee, D.; Seong, M.; Cha, C.; Jeong, H. E. Cellulose Acetate
11 1458 Nanoneedle Array Covered with Phosphorylcholine Moiety as a Biocompatible and
12 1459 Sustainable Antifouling Material. *Cellulose* **2019**, *26* (16), 8775–8788.
13 1460 <https://doi.org/10.1007/s10570-019-02681-w>.
- 14
15 1461 (93) Park, H.-H.; Sun, K.; Seong, M.; Kang, M.; Park, S.; Hong, S.; Jung, H.; Jang, J.; Kim, J.;
16 1462 Jeong, H. E. Lipid-Hydrogel-Nanostructure Hybrids as Robust Biofilm-Resistant Polymeric
17 1463 Materials. *ACS Macro Lett.* **2019**, *8* (1), 64–69.
18 1464 <https://doi.org/10.1021/acsmacrolett.8b00888>.
- 19
20 1465 (94) Choi, G.; Song, Y.; Lim, H.; Lee, S. H.; Lee, H. K.; Lee, E.; Choi, B. G.; Lee, J. J.; Im, S.
21 1466 G.; Lee, K. G. Antibacterial Nanopillar Array for an Implantable Intraocular Lens. *Adv.*
22 1467 *Healthc. Mater.* **2020**, *9*(18), 2000447. <https://doi.org/10.1002/adhm.202000447>.
- 23
24 1468 (95) Linklater, D. P.; Saita, S.; Murata, T.; Yanagishita, T.; Dekiwadia, C.; Crawford, R. J.;
25 1469 Masuda, H.; Kusaka, H.; Ivanova, E. P. Nanopillar Polymer Films as Antibacterial
26 1470 Packaging Materials. *ACS Appl. Nano Mater.* **2022**, *5* (2), 2578–2591.
27 1471 <https://doi.org/10.1021/acsanm.1c04251>.
- 28
29
30
31
32
33
34
35
36
37
38
39
40 1473
41
42
43
44
45
46
47
48
49
50
51
52
53
54
55
56
57
58
59
60